Whole-Cell Currents in Single and Confluent M-1 Mouse Cortical Collecting Duct Cells

CHRISTOPH KORBMACHER, ALAN S. SEGAL, GÉZA FEJES-TÓTH, GERHARD GIEBISCH, and EMILE L. BOULPAEP

From the Department of Cellular and Molecular Physiology, Yale University School of Medicine, New Haven, Connecticut 06510

ABSTRACT M-1 cells, derived from a microdissected cortical collecting duct of a transgenic mouse, grown to confluence on a permeable support, develop a lumen-negative amiloride-sensitive transepithelial potential, reabsorb sodium, and secrete potassium. Electron micrographs show morphological features typical of principal cells in vivo. Using the patch clamp technique distinct differences are detected in whole-cell membrane current and voltage (V_m) between single M-1 cells 24 h after seeding vs cells grown to confluence. (*a*) Under control conditions (pipette: KCl-Ringer; bath: NaCl-Ringer) V_m averages -42.7 ± 3.4 mV in single cells vs -16.8 ± 4.1 mV in confluent cells. Whole-cell conductance (G_{cell}) in confluent cells is 2.6 times higher than in single cells. Cell capacitance values are not significantly different in single vs confluent M-1 cells, arguing against electrical coupling of confluent M-1 cells. (*b*) In confluent cells, 10^{-4}–10^{-5} M amiloride hyperpolarizes V_m to -39.7 ± 3.0 mV and the amiloride-sensitive fractional conductance of 0.31 shows a sodium to potassium selectivity ratio of ~ 15. In contrast, single cells express no significant amiloride-sensitive conductance. (*c*) In single M-1 cells, G_{cell} is dominated by an inwardly rectifying K-conductance, as exposure to high bath K causes a large depolarization and doubling of G_{cell}. The barium-sensitive fraction of G_{cell} in symmetrical KCl-Ringer is 0.49 and voltage dependent. (*d*) In contrast, neither high K nor barium in the apical bath affect confluent M-1 cells, showing that confluent cells lack a significant apical K conductance. (*e*) Application of 500 μM glibenclamide reduces whole-cell currents in both single and confluent M-1 cells with a glibenclamide-sensitive fractional conductance of 0.71 and 0.83 in single and confluent cells, respectively. Glibenclamide inhibition occurs slower in confluent M-1 cells than in single cells, suggesting a basolateral action of this lipophilic drug on ATP-sensitive basolateral K channels in M-1 cells. (*f*) A component of the whole-cell conductance in M-1 cells appears as a deactivating outward current during large depolarizing voltage pulses and is abolished by extracellular chloride removal. The deactivating chloride current averages 103.6 ± 16.1 pA/cell, comprises 24% of the outward current, and decays with a time constant of 179 ± 13 ms.

Address correspondence to Dr. Christoph Korbmacher at his present address: Zentrum der Physiologie, Klinikum der Johann Wolfgang Goethe-Universität, Theodor Stern Kai 7, D-60590 Frankfurt am Main, Germany.

J. GEN. PHYSIOL. © The Rockefeller University Press · 0022-1295/93/10/0761/33 $2.00
Volume 102 October 1993 761–793

The outward to inward conductance ratio obtained from deactivating currents and tail currents is 2.4, indicating an outwardly rectifying chloride conductance.

INTRODUCTION

The mammalian cortical collecting tubule (CCT) plays an important role in the fine tuning of sodium reabsorption and potassium secretion. Many insights into the membrane properties and transport functions of CCT have been gained from in vitro electrophysiological studies of isolated perfused cortical collecting ducts (Frindt and Burg, 1972; O'Neil and Boulpaep, 1982; Schlatter and Schafer, 1987) and from studies at the single cell level in microdissected tubules (Koeppen, Biagi, and Giebisch, 1983; Hunter, Lopes, Boulpaep, and Giebisch, 1984; Frindt and Palmer, 1987, 1989; Sansom, La, and Carosi, 1990; Wang and Giebisch, 1991*a*,*b*).

Methods utilizing tissue culture have become an additional powerful tool to study renal epithelial function (Handler, Perkins, and Johnson, 1980). Examples of CCT tissue culture models previously used include several primary culture approaches using neonatal (Minuth and Kriz, 1982) or adult rabbit tissue (Spielman, Sonnenburg, Allen, Arend, Gerozissis, and Smith, 1986; Bello-Reuss and Weber, 1987). An important goal has been to develop a continuous mammalian CCT cell line which, under tissue culture conditions, expresses properties typical for CCT in vivo. Such a cell line should provide a continuous source of readily available cells with minimal variability between samples.

The M-1 cell line used in the present study was derived from a single microdissected cortical collecting duct of a mouse transgenic for the early region of simian virus 40, Tg(SV40)Bri/7. In mice transgenic for the early region of SV40, the genetic background is modified to enhance cell proliferation without losing the ability for differentiation (MacKay, Striker, Elliot, Pinkert, Brinster, and Striker, 1988). The M-1 cell line retains many antigenic and differentiated transport properties of the CCT. Antibody studies have shown that 75% of the cells express antigens characteristic for cortical collecting duct principal cells and some staining also occurs with antibodies directed against β-type intercalated cells (Stoos, Naray-Fejes-Tóth, Carretero, Ito, and Fejes-Tóth, 1991). When grown on permeable supports, the cells exhibit a high transepithelial resistance and a lumen negative transepithelial potential difference. The corresponding short-circuit current is sensitive to amiloride and is significantly increased by basolateral application of arginine vasopressin (Stoos et al., 1991).

The purpose of the present study is to characterize the electrophysiological properties of the M-1 cell line using whole-cell current measurements. Transepithelial electrical and ion gradient measurements were carried out in order to verify that M-1 cells express stable transport properties throughout the passages used in our whole-cell experiments. In whole-cell records we noticed marked differences between the currents in single M-1 cells and in M-1 cells from confluent monolayers. Amiloride-sensitive sodium channels are more abundant in confluent than in single cells. A glibenclamide-sensitive conductance was detected in the M-1 cells, which suggests the presence of ATP-sensitive potassium channels. Finally, large depolarizations activate a time-dependent outward current carried by chloride.

Part of this work was presented in abstract form (Korbmacher, Segal, Fejes-Tóth, Giebisch, and Boulpaep, 1991; Korbmacher, Segal, and Boulpaep, 1992)

MATERIALS AND METHODS

Cell Culture

The M-1 mouse cortical collecting duct cell line used in the present study was obtained from Dr. Fejes-Tóth and is of the same strain as previously described (Stoos et al., 1991). Cells were used from passage 6 to 14. Each passage was achieved with a split ratio of ~1:5 using 0.05% trypsin/0.53 mM EDTA in calcium- and magnesium-free HBSS (Gibco Laboratories, Grand Island, NY). Cells were grown in 100-mm Petri dishes which had been coated with rat tail collagen. Cells were maintained in a 5% CO_2 atmosphere at 37°C and the culture medium was exchanged twice per week. PC-1 culture medium (Ventrex, Portland, ME) was used and supplemented with 2 mM glutamine, 100 U/ml penicillin, and 100 μg/ml streptomycin. PC-1 medium is a low-protein, serum-free medium formulated in a specially modified DME:F-12 base. For patch clamp experiments, cells were seeded onto small rectangular pieces (~9 × 2.5 mm) of glass cover slips (Baxter Scientific Products, McGaw Park, IL). For transepithelial experiments cells were seeded onto permeable collagen membranes (Cellagen® Discs CD-24, ICN Biochemicals, Cleveland, OH) with an active surface area of 0.6 cm^2. Each cellagen® disc was placed in a separate well of a six-well culture dish (Corning, New York) containing 4 ml of culture medium (basolateral compartment). The apical compartment of each cellagen® disc was filled with ~400 μl of culture medium.

Transepithelial Electrical and Ion Gradient Measurements

Transepithelial potential difference (V_{te}) and resistance (R_{te}) were measured across M-1 cells grown on permeable collagen membranes (Cellagen® discs) using a commercially available epithelial volt/ohm meter and a set of two stick electrodes ('EVOM' and 'STX Electrodes'; World Precision Instruments, New Haven, CT). Measurements were performed under sterile conditions in a laminar flow cell culture hood. Thus, measurements could be repeated in an individual dish on several occasions. V_{te} was determined with reference to the basolateral solution compartment. The equivalent short circuit current (I_{sc}) was calculated as $I_{sc} = -V_{te}/R_{te}$. Apical and basolateral sodium and potassium concentrations were measured in 250 μl samples collected at the end of a feeding interval (i.e., 3 or 4 d after feeding the cells with fresh medium). The samples were analyzed by conventional flame photometry (Corning 480 Flame Photometer).

Patch Clamp Technique for Whole-Cell Current Recordings

The ruptured-patch whole-cell configuration of the patch clamp technique was used (Hamill, Marty, Neher, Sakmann, and Sigworth, 1981). Patch pipettes were fabricated from 100-mm borosilicate capillary tubes (Corning Glass 7052, ID = 1.2 mm, OD = 1.65 mm) using a two-stage vertical puller (PP-83, Narishige, Tokyo). Pipettes were coated with Sylgard 184® (Dow Corning Corporation, Midland, Michigan) and firepolished. Pipettes filled with standard pipette solution (for compositions of solutions see Table I) had resistances of 3–7 MΩ in NaCl-Ringer bath solution.

Experiments were performed in an elongated flow chamber (25 mm long, 5 mm wide, bath depth 2–4 mm) containing 250–500 μl of bath solution which was kept at 35 ± 2°C by an adjustable stream of heated air. The elongated design of the flow chamber permits rapid solution exchanges (within 5–10 s). The reference electrode was a Ag/AgCl pellet bathed in the

same solution as that used in the pipette, and connected to the bath via a 3-M KCl agar bridge positioned in the outflow path of the flow channel. Cells were observed using an inverted microscope (Reichert Biovert, Vienna, Austria) equipped with Hoffman modulation optics (Modulation Optics Inc., Greenvale, NY). The patch pipette was held on a motor-driven Huxley-style micromanipulator (Model MX300R, Newport Bio-Instruments, Mountain Valley, CA).

Membrane currents were detected with a List EPC-7 patch/whole cell clamp amplifier (List Electronic, Darmstadt, Germany). Whole-cell currents were recorded using the voltage clamp mode (VC) and filtered at 10 kHz. Membrane voltage V_m was observed by switching from VC to zero current clamp (CC) mode. Whole-cell currents and holding potential V_{hold} (or V_m in CC-mode) were continuously recorded on a Gould 2400 Recorder (Gould Inc., Cleveland, Ohio).

The membrane current resulting from voltage stimuli was sampled at a rate of 375/s and stored directly on the hard disk (Data System Design DSD 880D/30, San Jose, CA). Voltage clamp commands, data acquisition during voltage step protocols, and data analysis were

TABLE I

Solution composition

in mM	NaCl Ringer	KCl Ringer	K-cyclamate Ringer	Na-cyclamate Ringer	Pipette solution
Na^+	145	5	5	145	5
K^+	5	145	145	5	145
Ca^{2+}	1	1	1	1	—
Mg^{2+}	1	1	1	1	1
Cl^-	149	149	9	9	149
$Cyclamate^-$	—	—	140	140	—
$Hepes^-$	5	5	5	5	5
Hepes	5	5	5	5	5
Glucose	5	5	5	5	—
EGTA	—	—	—	—	1

The pH of the solutions was adjusted to 7.5 using 1 *N* NaOH or KOH depending on whether the dominant cation of the solution was sodium or potassium, respectively.

controlled by a PDP 11/23 computer with a Cheshire interface and HP-1345A digital display (Indec Systems, Sunnyvale, CA). Data were plotted using a HP 7470A digital plotter (Hewlett-Packard, San Diego, CA). Software for voltage stimulation, current sampling, data acquisition and analysis was written or adapted by A. S. Segal.

After successful cell-attached giga-ohm (GΩ) seal formation, the patch membrane was ruptured by additional suction to achieve the conventional whole-cell configuration. At this stage, the membrane capacitance (C_m) and the series resistance (R_s) were digitally computed online from the capacitive transient. This transient was then nulled using the analog circuitry within the patch-clamp amplifier and estimates of the membrane capacitance, C_m and the series resistance, R_s were read from the corresponding knob settings on the EPC-7. In experiments in which both methods were used, good agreement was obtained between the readings of the knob settings (R_s = 24.83 ± 7.66 MΩ; C_m = 14.60 ± 2.36 pF) and the values calculated from the transients (R_s = 25.97 ± 6.48 MΩ; C_m = 14.61 ± 2.03 pF), and there was no significant difference when the data were compared using the paired *t*-test (n = 11). In 56 experiments, R_s averaged 23.6 ± 2.57 MΩ. We were unable to further reduce R_s because it was difficult to

obtain seals with lower resistance pipettes (<3 MΩ). The R_s compensation circuitry of the EPC-7 was not used in order to avoid the possibility of amplifier oscillations. Thus, for a typical whole-cell current of 200–400 pA and an R_s of 25 MΩ, the voltage error for V_{hold} would be 5–10 mV. The effect of this R_s on the frequency response is negligible at a sampling rate of 375/s.

Routinely cells were held at a holding potential (V_{hold}) of −60 mV and 400 ms step pulses to 0 mV were given every 2 s. The overall cell conductance G_{cell} was estimated by calculating $G_{cell} = \Delta I/60$ mV where ΔI is the whole-cell (peak) current deflection observed upon stepping V_{hold} from −60 mV to 0 mV.

Solutions and Chemicals

The composition of the solutions is given in Table I. In some experiments, the pipette-solution was KCl-Ringer to which 10 mM EGTA was added in order to reduce the free calcium concentration to $<10^{-8}$ M. Amiloride hydrochloride was a gift from Merck Sharp and Dohme (Rahway, NJ) and glibenclamide was obtained from Sigma Chemical Co. (St. Louis, MO). Glibenclamide was dissolved in 0.05 N KOH for use in KCl-Ringer (or NaOH when used in NaCl-Ringer) and a 25-mM glibenclamide stock solution was freshly prepared the day of the experiment.

RESULTS

Cell Culture

When grown on a nonpermeable support, M-1 cells form 'domes' after reaching confluence. Fig. 1 shows phase contrast micrographs of a 6-d old M-1 cell culture with typical 'dome' formation. Fig. 2 *A* shows a transmission electron micrograph of M-1 cells grown on a permeable cellagen® support. Cells are cuboidally shaped with prominent tight junctional complexes along the apical membrane cell borders. The cytoplasm of the cells stains lightly with few organelles in the apical cytoplasm and few mitochondria throughout the cell. The basolateral infoldings of the cells are not extensive but are elongated, often extending across the intercellular space which exhibits only a small degree of dilation. The basal lamina is simple and smooth and remains in contact with the culture surface. The apical membrane is decorated with short microvilli and often a short central cilium is found. Fig. 2 *B* shows M-1 cells grown to confluence on glass cover slips. They maintain microvilli on their apical membrane and develop tight junctions. The intercellular spaces are wider in cultures grown on glass than in those on permeable support, probably as a result of fluid reabsorption against a nonpermeable barrier. The upper inset of Fig. 2 *B* shows a central cilium at higher magnification; its electron dense rootlet extends into the cytoplasm. The lower inset shows a scanning electron micrograph confirming the microvillar structure of the apical membrane and central placement of the singular cilium. The electron micrographs show no evidence of more than one cell type in M-1 cell cultures. Fig. 2 *C* shows a single M-1 cell 24 h after seeding on a glass cover slip.

Transepithelial Measurements

Within a week after seeding, M-1 cell monolayers develop lumen negative transmonolayer potential differences ranging from −12 to −48 mV and transmonolayer electrical resistances ranging from 200 to 900 Ω cm^2. In 44 individual cultures, V_{te}

averaged -28.8 ± 1.4 mV, R_{te} was $550.5 \pm 23.0\ \Omega\ cm^2$ and the calculated equivalent I_{sc} averaged $54.0 \pm 3.0\ \mu A\ cm^{-2}$. The lumen negative transmonolayer potential and the high transepithelial electrical resistance was a stable characteristic of M-1 cells throughout the passages used (passages 7–14).

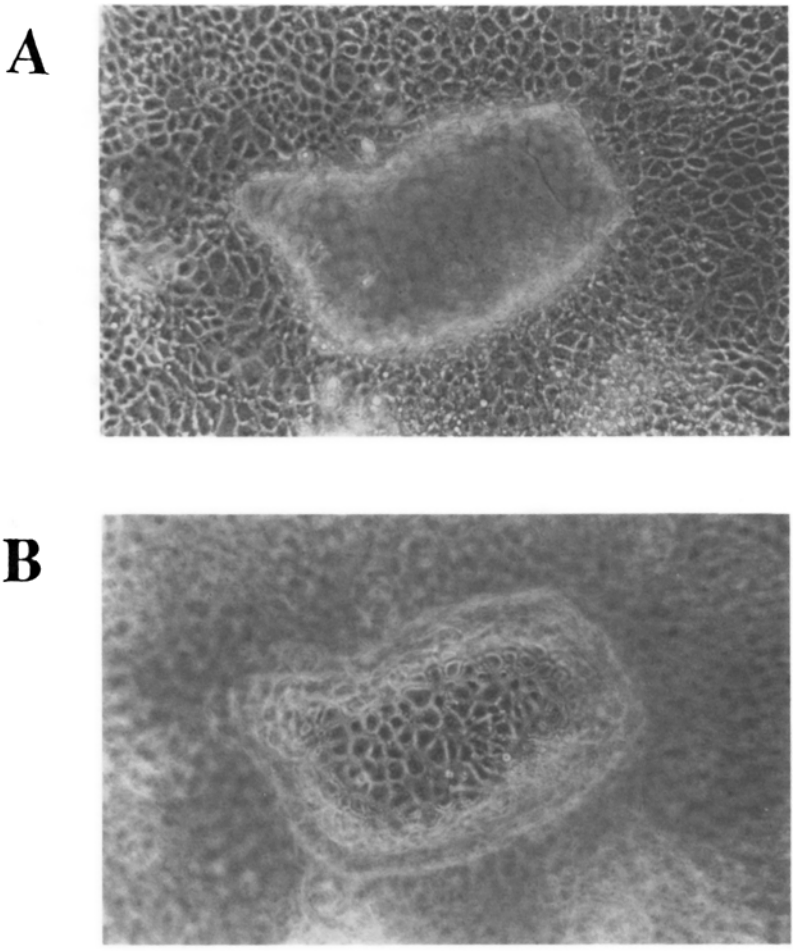

FIGURE 1. Phase contrast micrograph of a 6-d old M-1 cell culture demonstrating 'dome' formation. (*A*) Focussed at the cell monolayer attached to the bottom of the dish; (*B*) same area but focussed at the top of a fluid-filled blister, or 'dome.'

Experiments were performed to investigate the effect of the apical application of amiloride on V_{te}, R_{te}, and on the sodium and potassium gradients established within a feeding interval. Apical and basolateral medium samples were obtained at the end of a 3–4-d feeding interval and sodium and potassium concentrations were measured.

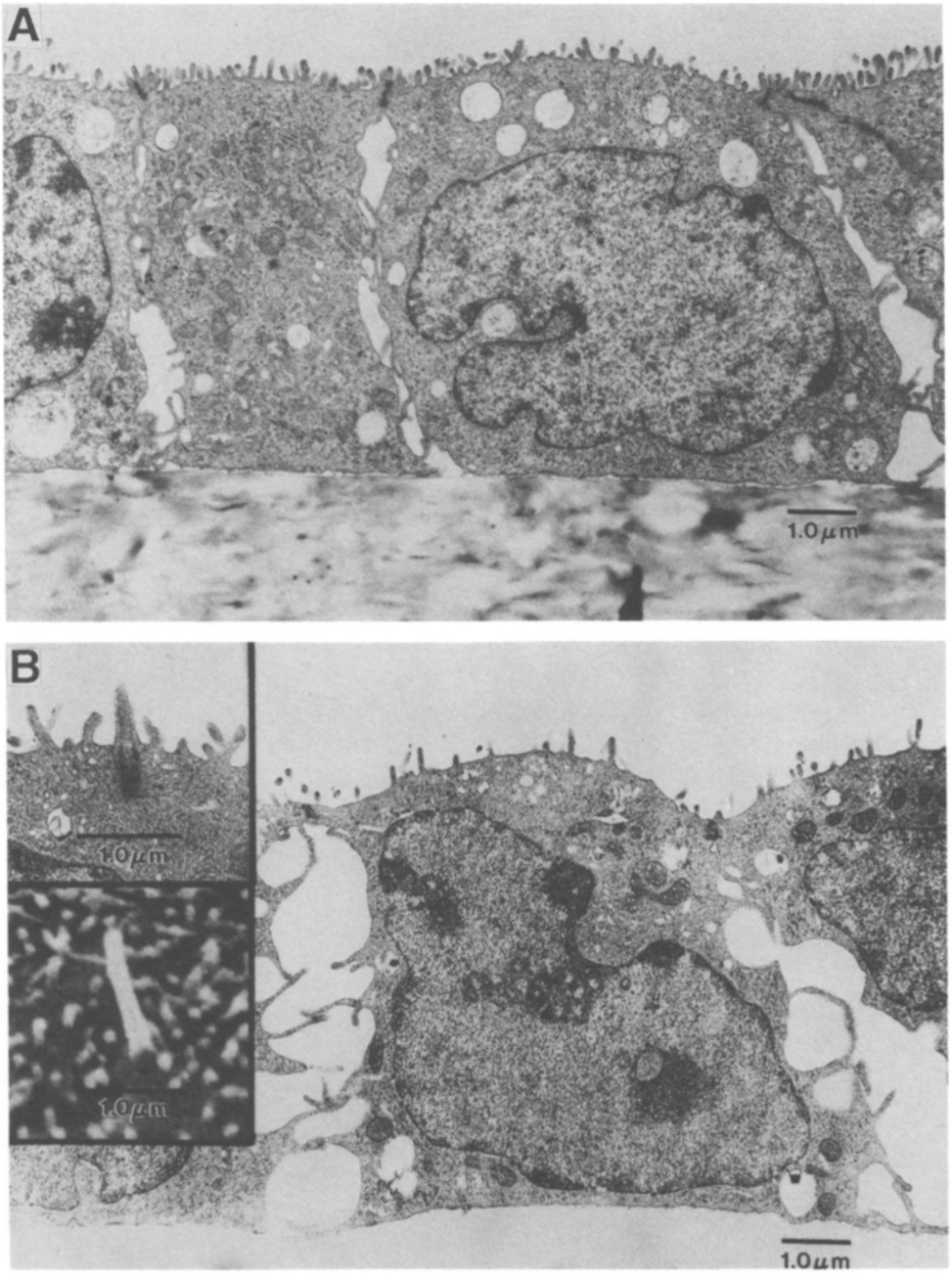

FIGURE 2.

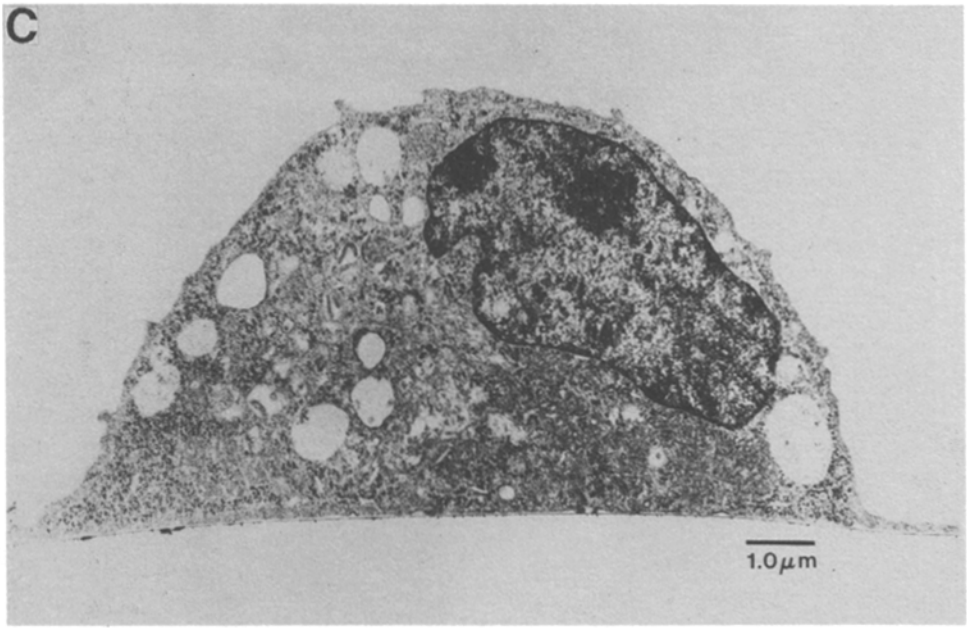

FIGURE 2. Transmission electron micrographs of M-1 cells. (*A*) Cells grown to confluence on permeable cellagen® support. (*B*) Cells grown to confluence on glass. Upper inset shows a transmission electron micrograph and lower inset a scanning electron micrograph of a central cilium at higher magnification. (*C*) Single M-1 cell 24 h after seeding on glass.

Transepithelial electrical measurements were made 1–2 h after feeding the confluent monolayers with fresh medium. Subsequently, one set of cells was exposed to 10 μM amiloride applied from the apical side and the acute effect of amiloride on V_{te} and R_{te} was determined. At the end of the 3–4 day feeding interval, measurements were

TABLE II

Effect of Amiloride on V_{te}, R_{te}, and I_{sc} in M-1 Cell Monolayers

	V_{te}(mV)	R_{te}(Ωcm²)	I_{sc}(μAcm⁻²)
	Control group (n = 5)		
Day 0	−25.5 ± 2.2	707.0 ± 82.2	38.5 ± 5.7
Day 3–4	−10.7 ± 1.1	308.5 ± 19.6	34.5 ± 1.8
	Amiloride group (n = 10)		
Day 0: prior amiloride	−28.6 ± 2.2	637.6 ± 44.8	47.9 ± 5.6
Day 0: 10 μM amiloride	−1.7 ± 0.4	926.3 ± 43.8	1.7 ± 0.5
Day 3–4 with amiloride	−3.0 ± 0.9	653.5 ± 36.9	5.1 ± 1.5

Initial values were measured 1–2 h after feeding the cells with fresh PC1-medium. Subsequently, 10 μM amiloride were added to the apical compartment of the culture dishes in the amiloride group and measurements were repeated in the presence of amiloride. The final values were obtained 3–4 d later just before obtaining the samples for the sodium and potassium concentration measurements (see Table III). The culture medium had not been changed during this time interval (which corresponds to a normal feeding cycle) and amiloride was continuously present in the cultures of the amiloride group.

repeated before taking samples for the ion concentration measurements. Data from four independent sets of experiments are summarized in Tables II and III. Cells were from passages 7 and 10 and were studied 3–16 d after seeding.

The experiments demonstrate that application of amiloride depolarizes V_{te}, increases R_{te} and in turn nearly abolishes I_{sc}, indicating electrogenic amiloride-sensitive sodium reabsorption (Table II). This is further supported by the ion gradient measurements (Table III), which show that within a feeding cycle the cells establish a basolateral (*bl*) to apical (*ap*) concentration ratio of $[Na]_{bl}/[Na]_{ap}$ of 1.21 under control conditions and a ratio of 1.06 in the presence of amiloride ($p < 0.001$). The ratio of 1.21 corresponds to an E_{Na} of +5.1 mV (lumen positive). In the presence of a lumen negative transepithelial potential, this demonstrates active sodium reabsorption under control conditions.

TABLE III

Effect of Amiloride on Ion Concentrations in the Apical and Basolateral Compartments of M-1 Cell Monolayer Cultures

	Control group (n = 5)	Amiloride group (n = 10)
$[Na^+]_{bl}$	150.2 ± 1.7 mM	144.9 ± 1.4 mM
$[Na^+]_{ap}$	124.2 ± 2.4 mM	136.6 ± 2.2 mM
$[Na^+]_{bl}/[Na^+]_{ap}$	1.21 ± 0.01	1.06 ± 0.01
E_{Na}	+5.1 ± 0.3 mV	+1.6 ± 0.3 mV
$[K^+]_{bl}$	4.51 ± 0.15 mM	4.63 ± 0.11 mM
$[K^+]_{ap}$	8.27 ± 0.15 mM	6.05 ± 0.09 mM
$[K^+]_{bl}/[K^+]_{ap}$	0.55 ± 0.02	0.77 ± 0.03
E_K	−16.3 ± 0.9 mV	−7.2 ± 1.0 mV

Same experiments as in Table II. Sodium and potassium concentrations were determined in the apical and basolateral culture medium of M-1 cells at the end of a 3–4-d feeding interval. In the amiloride group, 10 μM amiloride was present in the apical medium throughout the experiment. Equilibrium potentials E_K (and E_{Na}) were calculated for each pair of measured apical and basolateral potassium (sodium) concentrations according to the equations:

$$E_K = 61.55 \text{ mV} * \log ([K^+]_{bl}/[K^+]_{ap})$$
$$E_{Na} = 61.55 \text{ mV} * \log ([Na^+]_{bl}/[Na^+]_{ap}).$$

Table III demonstrates that under control conditions a potassium gradient is established across the monolayer with a ratio $[K^+]_{bl}/[K^+]_{ap}$ of 0.55, corresponding to an E_K of −16.3 mV (lumen negative). This value falls within the range of V_{te} measured at the beginning (−25.5 mV) and at the end (−10.7 mV) of the feeding cycle (Table II). Thus, under control conditions the potassium gradient across the monolayer is compatible with a passive distribution predicted by the transepithelial potential difference. However, in the presence of 10^{-5} M amiloride the ratio $[K^+]_{bl}/[K^+]_{ap}$ is 0.77 (Table III). The corresponding E_K value of −7.2 mV is significantly more negative than the V_{te} values measured directly after addition of amiloride ($p < 0.001$) or at the end of the feeding cycle in the continuous presence of amiloride ($p < 0.01$, Table II). Passive distribution alone cannot account for the transepithelial potassium gradient established in the presence of amiloride. Thus, M-1 cells grown on a permeable support actively secrete potassium.

Whole-Cell Current Measurements in M-1 Cells

Following giga-ohm seal formation, conventional whole-cell patch configurations were obtained in single, 1-d old M-1 cells and in 5–14-d old M-1 cells which had formed a monolayer and displayed domes. In preliminary studies carried out at room temperature, the success rate of seal formation on confluent cells was low. At 35°C, giga-seals were readily obtained on single M-1 cells in about one out of two attempts, and on confluent cells in about one out of five attempts. After successful giga-seal formation, the whole-cell configuration was achieved in ~50% of the attempts. Cells were bathed in control NaCl-Ringer and the patch pipette contained 145 mM KCl. The average values for G_{cell}, V_m, and C_m measured within the first minute after achieving the whole-cell configuration are shown in Table IV. Confluent cells have a significantly larger G_{cell} and a significantly less negative membrane voltage than single cells. Cell capacitance is not significantly different in confluent and single cells (Table IV). As evidenced by large SE-values (Table IV) the measured whole-cell currents varied considerably from cell to cell ranging over an order of magnitude even in the same batch of cells. This wide scatter is similar to that reported for whole cell current

TABLE IV

Comparison of G_m, V_m, and C_m of Single and Confluent M-1 Cells

M-1 cells	V_m	C_m	G_{cell}
	mV	pF	*nS*
Single	−42.7 ± 3.4	11.7 ± 1.1	2.81 ± 0.64
	n = 30	n = 25	n = 29
Confluent	−16.8 ± 4.1	13.7 ± 1.4	7.33 ± 0.96
	n = 26	n = 19	n = 26
p <	0.001	n.s.	0.001

n.s., not significantly different in unpaired *t*-test.

measurements in rat cortical collecting duct principal cells (Frindt, Sackin, and Palmer, 1990).

Giga seals could usually be maintained from several minutes up to more than half an hour. This made it possible to perform solution exchanges and to apply drugs while continuously monitoring G_{cell} (in VC mode) or V_m (in CC mode). However, during the course of prolonged experiments large spontaneous fluctuations (decreases as well as increases) of G_{cell} and V_m were not uncommon. Thus, when ion substitution or drug effects on V_m or G_{cell} were tested, measurements obtained just before the experimental period served as controls. The explanation for the spontaneous slow fluctuations in the whole cell conductances which occur over several minutes is not clear, but may be related in part to washout of intracellular substances. ATP and PKA have recently been shown to prevent K-channel rundown in excised patches from the apical membrane of rat cortical collecting duct cells (Wang and Giebisch, 1991*a*). In preliminary experiments in which we added to the pipette solution 0.1 mM ATP alone (n = 2) or together with 25 U/ml of catalytic subunit of protein kinase A (n = 4), we did not notice a qualitatively different behavior of the

whole-cell currents. In confluent monolayers, a varying degree of cell to cell coupling could theoretically account for changes in the whole cell conductances during an experiment. However, conductance fluctuations were also observed in single cells and little or no cell to cell coupling has been shown to occur between cortical collecting duct cells in situ (Frindt et al., 1990).

Whole-Cell Current Measurements in 1-d-old Single M-1 Cells

Effect of amiloride on single M-1 cells. In the presence of 10^{-5} M amiloride, G_{cell} averages 1.76 ± 0.54 nS compared to 1.89 ± 0.56 nS in the same cells in Na-Ringer in the absence of amiloride (n = 9, not significantly different in paired t-test). The V_m in the presence of 10^{-5} M amiloride averages −42.4 ± 7.4 mV and is slightly more negative than the average V_m of −39.4 ± 7.3 mV in the same cells under control conditions (n = 10, $p < 0.01$ in paired t-test). The small hyperpolarization caused by

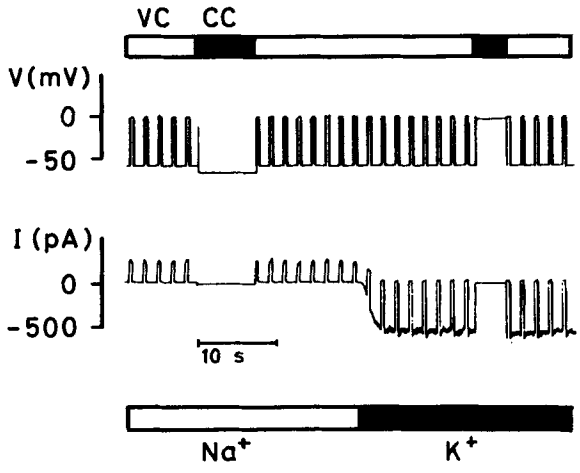

FIGURE 3. Continuous whole-cell recording in a single M-1 cell, one day after seeding, either in voltage clamp (*VC*) mode or current clamp (*CC*) mode (*upper bar*). *V* indicates the holding potential in VC mode and the membrane voltage in CC mode, respectively. In VC mode, the holding potential was stepped every 2 s from −60 mV to 0 mV for 400 ms. Whole-cell current *I* shows inward current as negative. The lower bar indicates changes in superfusion solution from NaCl-Ringer (*open bar*) to KCl-Ringer (*solid bar*).

amiloride is compatible with inhibition of a modest amiloride-sensitive sodium conductance.

Exposure of single M-1 cells to KCl-Ringer. Fig. 3 shows a trace from an experiment on a single M-1 cell in which the bath solution was changed from control NaCl-Ringer to KCl-Ringer. Under voltage clamp conditions the holding potential was stepped every 2 s from −60 to 0 mV for 400 ms. In the presence of NaCl-Ringer, almost no current was observed at V_{hold} = −60 mV, but outward current was seen when the holding potential was stepped to 0 mV. The cell conductance under these conditions was 4.2 nS and the membrane voltage recorded at zero current clamp was −68 mV. When the bath solution was changed to KCl-Ringer a significant inward current was observed at V_{hold} = −60 mV. At V_{hold} = 0 mV minimal current was measured, verifying that both cytoplasm and bath contain KCl-Ringer. Changing the bath from NaCl-Ringer to KCl-Ringer increased G_{cell} by 148% to 10.4 nS and

depolarized V_m to −2.8 mV. Overall, the conductance increase due to a change from NaCl-Ringer to KCl-Ringer averages 116% from 1.81 ± 0.3 nS to 3.91 ± 0.70 nS (n = 19, p < 0.001 in paired t-test) and V_m depolarizes from −34.1 ± 4.1 mV to −0.3 ± 0.3 mV (n = 19, p < 0.001 in paired t-test).

The increase in G_{cell} in a KCl-Ringer bath is smaller in cells starting with a less negative membrane voltage in control NaCl-Ringer. Fig. 4 illustrates the correlation between membrane potential and the G_{cell} response to elevation of $[K]_o$ from 5 to 145 mM, expressed as $(G^{145K} - G^{145Na})$ normalized to G^{145K}. This relationship shows that cells with less negative membrane voltages under control conditions have a smaller relative K-conductance than cells with more negative membrane voltages closer to the E_K of −90 mV.

Figs. 5 and 6 show current traces and I/V plots obtained from voltage step protocols applied to a whole-cell patch while the bath solution was changed from control NaCl-Ringer to KCl-Ringer. It is noteworthy that the current traces generated by voltage steps more positive than 30 mV (Figs. 5 *A* and 6 *A*) show time-dependent decay during the 400-ms pulse. This is also reflected by the different shapes of the

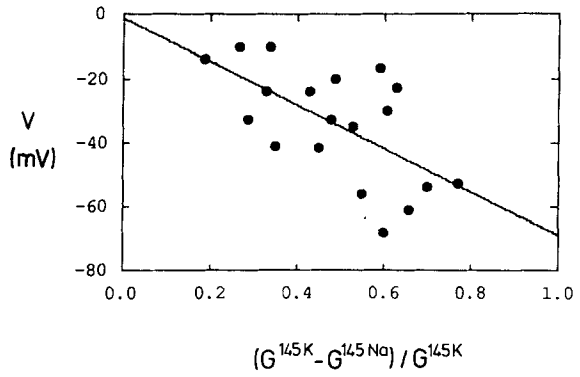

FIGURE 4. Correlation between membrane potential (V) and G_{cell} response to elevation of the extracellular potassium concentration from 5 to 145 mM, expressed as $(G^{145K} - G^{145Na})$ normalized to G^{145K}. Experiments were performed in single M-1 cells one day after seeding. Data are fitted by linear regression analysis (r = 0.62, n = 19).

I/V plots in Figs. 5 *B* and 6 *C* which were obtained by sampling and averaging the current data points during the early portion (5–16 ms into the pulse) and the late portion (387–397 ms) of the current traces. Whereas during the initial period the outward slope appears to be linear, the I/V plots obtained at the end of the pulses show a bend starting at +60 mV, which is most pronounced at +90 mV.

In control NaCl-Ringer (Fig. 5 *A*) the zero current potential (E_{rev}) on the I/V plots is close to the V_m of −58 mV measured in CC-mode before switching to VC-mode. Accordingly, very little inward current is detected at the holding potential of −60 mV.

In the presence of KCl-Ringer, the reversal potential shifts to 0 mV and the inward current at −60 mV increases considerably (Fig. 6). When the early current measurements (5–16 ms) are used to calculate the chord conductance between −90 and 0 mV (G^{early}_{-90}) and the chord conductance between +90 and 0 mV (G^{early}_{+90}), the inward and outward conductance are not significantly different (G^{early}_{-90} = 4.53 ± 0.99 nS and G^{early}_{+90} = 4.44 ± 0.77 nS). The early (5–16 ms) inward to outward current ratio averaged 0.96 ± 0.10 (n = 13 measurements from I/V plots obtained from six different cells). In contrast, when the late current measurements (387 to 397 ms) in

the same experiments are used to calculate the corresponding chord conductances (G^{late}_{-90} and G^{late}_{+90}), the inward conductance averages G^{late}_{-90} = 4.41 ± 0.95 nS as compared to the outward conductance which averages G^{late}_{+90} = 3.35 ± 0.64 nS (n = 13 measurements, $p < 0.05$). This corresponds to a late (387–397 ms) inward to outward conductance ratio of 1.22 ± 0.12, significantly different from the initial ratio of 0.96 ± 0.10 ($p < 0.001$). Thus, inward rectification is observed at the end of the pulse.

Time-dependent decay of the outward current. Fig. 6 *B* represents the resultant average of four consecutive current traces induced by voltage pulses of −60 to +90 mV. During the 400-ms of sustained depolarization there is a time-dependent decay

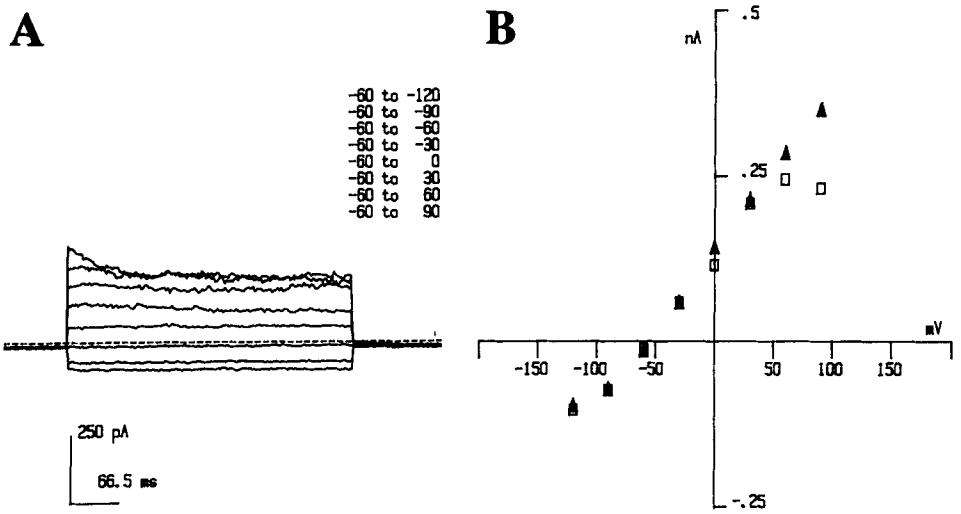

FIGURE 5. Whole-cell current traces (*A*) and I/V plots (*B*) obtained from voltage step protocols on a single M-1 cell in a NaCl-Ringer bath. (*A*) Average current traces obtained during four consecutive voltage step protocols, from a holding potential of −60 mV and starting with the hyperpolarizing pulse to −120 mV, as indicated in the inset. Pulse duration of 400 ms. After each pulse the holding potential was returned to −60 mV for ~1 s. Dashed line indicates zero current. (*B*) I/V plots obtained from the traces in *A*, by sampling and averaging the current traces during the early portion (5 to 16 ms into the pulse, *solid triangles*) and the late portion (387–397 ms into the pulse, *open squares*).

of the outward current. This relaxation of current cannot be due to activation of an inward current component because at a command potential of +90 mV the net driving force for K^+, Na^+, and Cl^- currents is outward. The apparent deactivation of the outward current can be fitted by a single exponential function with a time constant of 170 ms (Fig. 6 *B*). The peak current is reached instantaneously (within the sampling interval of 2.7 ms), suggesting that channels responsible for this current are not activated by depolarization. Upon return to the holding potential of −60 mV after the depolarization the inward tail current is reduced. The decreased tail current also indicates that channel inactivation has occurred during the 400 ms command pulse. During the 1.6-s post-pulse interval the inward current recovers to the

pre-depolarization level, indicating a reactivation of the conductance at the holding potential of −60 mV.

The amplitude of the current decay (I_{out}) was assessed by subtracting the late from the initial outward current during a 400-ms step pulse from −60 to +90 mV. The average current data from the first 5–16 ms of a pulse ($I_{(5-16)}$) and from the last 387–397 ms of the same pulse ($I_{(387-397)}$) were used to calculate $\Delta I_{out} = I_{(5-16)} -$

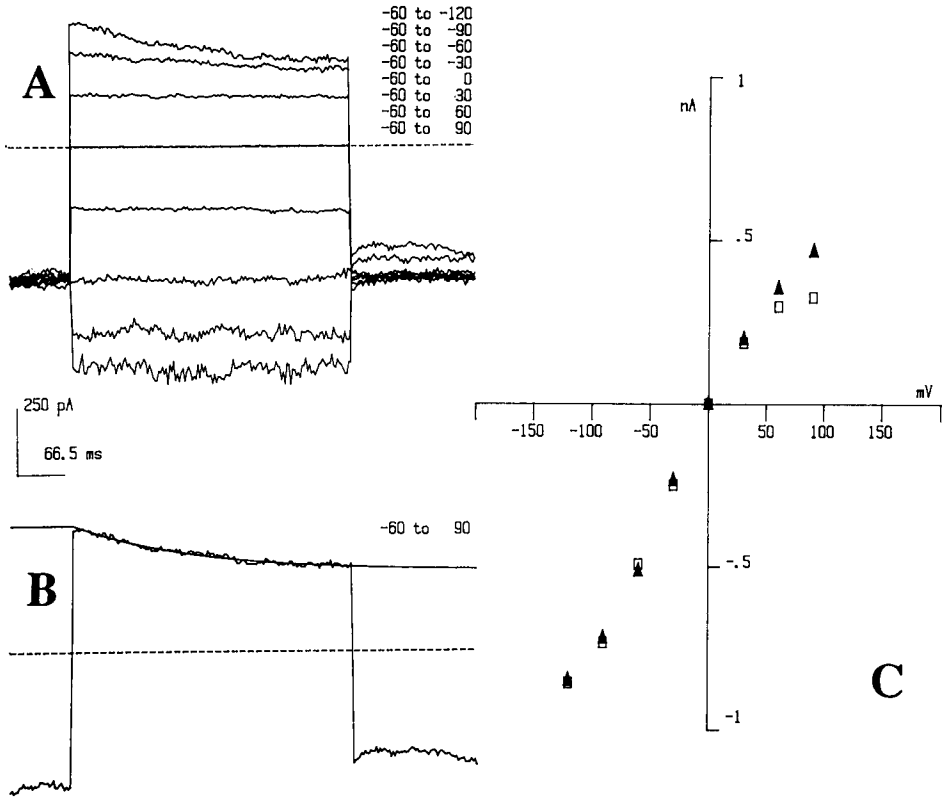

FIGURE 6. Whole-cell current traces (*A* and *B*) and I/V plots (*C*), obtained from voltage step protocols on the same cell as in Fig. 5, but 2.5 min later and after changing the bath from NaCl-Ringer to KCl-Ringer. (*A* and *C*) Voltage step protocol and symbols are the same as in Fig. 5. (*B*) Average of four current traces in response to a voltage pulse from −60 to +90 mV. The deactivation of the outward current is fitted by a single exponential with a time constant τ = 170 ms.

$I_{(387-397)}$. The decaying component of the outward current at +90 mV averages ΔI_{out} = 103.6 ± 16.1 pA corresponding to 24.1 ± 2.6% of the total outward current (n = 23). As shown in Table V, the magnitude of ΔI_{out} is not significantly different when cells are bathed either in NaCl-Ringer or in KCl-Ringer or in KCl-Ringer in the presence of 2 mM barium. The time constant of the current decay is also independent of the bath and averages τ = 179.1 ± 13.4 ms (Table V). Calculation of the

chord conductance ($\Delta G_{out} = \Delta I_{out}/90$ mV) shows that the decaying component of the outward conductance averages $\Delta G_{out} = 1.15 \pm 0.18$ nS ($n = 23$).

Tail currents were averaged 5–16 ms after the step from +90 to −60 mV (I_{after}) and the corresponding inward currents were averaged 7–17 ms before the step from −60 to +90 mV (I_{before}). In 12 out of 23 averaged current traces, I_{after} was more positive than I_{before}, and was followed by a time-dependent increase of the inward current as shown in Fig. 6 *B*. In the other traces, a tail current could not be resolved, either

TABLE V

Inactivation of Outward Current

Bath	Magnitude ΔI_{out}*	Relative magnitude ΔI_{out}%‡	Time constant τ§
	pA	%	ms
NaCl-Ringer	107.9 ± 26.4 (n = 7)	23.7 ± 5.6 (n = 7)	153.0 ± 38.8 (n = 5)
KCl-Ringer	99.4 ± 24.6 (n = 13)	25.1 ± 3.3 (n = 13)	186.4 ± 14.0 (n = 10)
KCl-Ringer 2 mM Ba^{2+}	111.5 ± 35.5 (n = 3)	20.5 ± 7.3 (n = 3)	198.4 ± 18.8 (n = 3)
Cumulative values	103.6 ± 16.1 (n = 23)	24.1 ± 2.6 (n = 23)	179.1 ± 13.4 (n = 18)

*The magnitude of the outward current decay (ΔI_{out}) was calculated from the initial current values ($I_{(5-16)}$ at 5–16 ms) and the late current values ($I_{(387-397)}$ at 387–397 ms) measured during 400 ms depolarizing pulses from −60 to +90 mV according to:

$$\Delta I_{out} = I_{(5-16)} - I_{(387-397)}.$$

‡The relative magnitude of the outward current decay (ΔI_{out}%) was calculated according to:

$$\Delta I_{out}\% = (\Delta I_{out}/\Delta I_{(5-16)}) \times 100.$$

§The time constant (τ) was obtained from single exponential fits of the current traces between 5 and 397 ms.

Averaged current traces of at least four subsequent pulses (−60 to +90 mV) were used to measure $I_{(5-16)}$ and $I_{(387-397)}$ and for the fitting procedure. For each experimental condition (Na-Ringer, K-Ringer, K-Ringer 2 mM Ba^{2+}) measurements were obtained from three to six different cells. In a number of experiments, more than one reading was obtained from the same cell (subsequent exposures to several bath solutions). Values are given as mean ± SEM and n indicates number of measurements (or fits) which were averaged.

because the difference may have been too small or masked by capacitance undercompensation. In the 12 current traces analyzed, the difference values $\Delta I_{in} = I_{before} - I_{after}$ were used to calculate the time-dependent component of the inward conductance ($\Delta G_{in} = \Delta I_{in}/-60$ mV), which averages $\Delta G_{in} = 0.59 \pm 0.14$ nS ($n = 12$ measurements). In the same traces, the time-dependent component of the outward conductance ΔG_{out} averages 1.42 ± 0.28 nS ($n = 12$, $p < 0.01$). Assuming that inactivation of the same conductance is responsible for the outward current decay

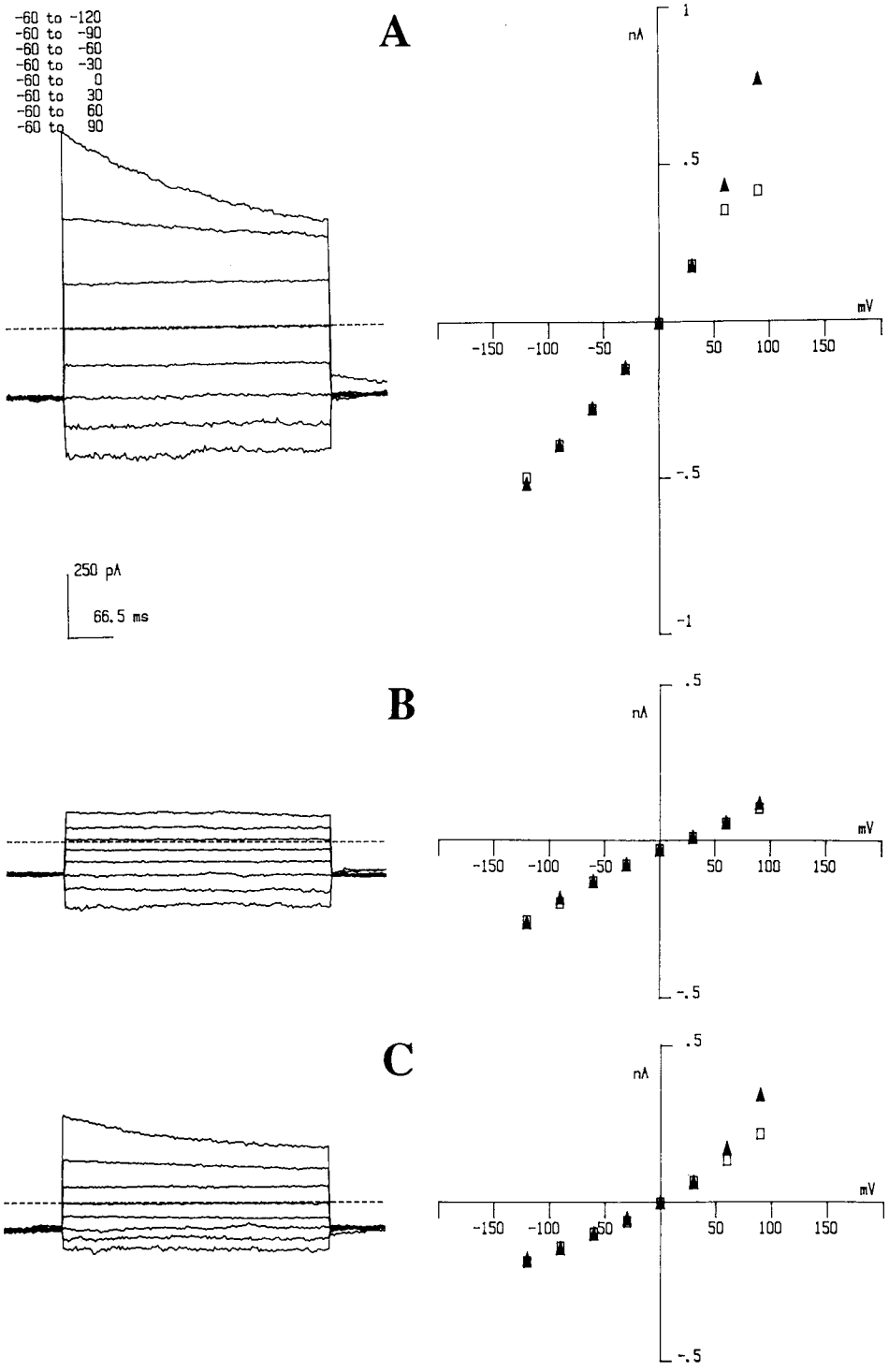
-60 to -120
-60 to -90
-60 to -60
-60 to -30
-60 to 0
-60 to 30
-60 to 60
-60 to 90
250 pA
66.5 ms
A
B
C
nA
mV
1
.5
-.5
-1
-150
-100
-50
50
100
150

FIGURE 7.

and the reduced tail currents, the ratio $\Delta G_{out}/\Delta G_{in}$ of 2.4 suggests that the underlying conductance exhibits outward rectification.

Effect of Cl^- removal on the outward current. Under the experimental conditions of Fig. 6, outward currents may be carried either by potassium ions leaving the cell or by chloride ions entering the cell. To test the hypothesis that the time dependent portion of the outward current is carried by chloride ions, extracellular chloride was replaced by using either Na-cyclamate or K-cyclamate Ringer.

In the experiment shown in Fig. 7, time dependent inactivation of outward current in the presence of symmetrical potassium and chloride concentrations was particularly pronounced (decaying portion 45.5% of early outward current). The early I/V plot obtained from the first 5–16 ms of the pulse shows considerable outward rectification, whereas the late I/V plot shows slight inward rectification (Fig. 7 *A*, *right*). It is noteworthy that in this cell V_m was only −16 mV in a control NaCl-Ringer bath and that the conductance increases only 37.5% when the bath is changed to KCl-Ringer. These findings are compatible with the presence of a relatively large chloride conductance in this cell.

As shown in Fig. 7 *B* changing extracellular chloride concentration from 149 mM (KCl-Ringer) to 9 mM (K-cyclamate-Ringer) almost completely abolishes the time-dependent portion of the outward current, indicating that the relaxation of the outward current is indeed due to a decaying chloride conductance. In the presence of K-cyclamate Ringer early and late I/V plots are practically identical (Fig. 7 *B*, *right*).

The effect of chloride removal on the time-dependent deactivation is reversible (Fig. 7 *C*). KCl-Ringer in the bath restores the disparity between initial and late I/V plots (Fig. 7 *C*, *right*), similar to the I/V plots before chloride removal. However, cell membrane conductance had declined by more than 50% during the experiment (compare Fig. 7, *A* with *C*). An overall loss of cell conductance with time may explain why changing from KCl-Ringer to K-cyclamate Ringer reduces not only the outward current but also affects the inward current. This spontaneous "run-down" of the cell conductance is not readily explained, because the concentrations of the principal ions carrying inward current (i.e., $[K^+]_o$ and $[Cl^-]_i$) are unchanged. As noted above, spontaneous fluctuations of G_{cell} and V_m were not uncommon during prolonged experiments. A nonspecific effect of cyclamate cannot be ruled out. In fact, in four out of five experiments in which cells were exposed to cyclamate, a subsequent continuous decrease of overall conductance was noted.

The time-dependent decay of currents during depolarizing voltage pulses was also abolished in experiments when the extracellular solution was changed from control Na-Ringer to Na-cyclamate Ringer ($n = 2$). In these two experiments and in three experiments with K-cyclamate Ringer (as shown in Fig. 7) the ΔI_{out} averages 2.8 ± 3.7 pA ($\Delta I_{out}\% = 2.2 \pm 10.3\%$, $n = 5$, not significantly different from zero). In these same experiments ΔI_{out} averages 144.4 ± 62.5 pA ($\Delta I_{out}\% = 26.9 \pm 8.8\%$, $n = 5$, $p < 0.05$) before the exposure to cyclamate Ringer and 69.3 ± 22.4 pA

Figure 7 (*opposite*). Whole-cell current traces and I/V plots obtained from voltage step protocols on a single M-1 cell one day after seeding. Voltage step protocol and symbols are the same as in Fig. 5. (*A*) In symmetrical KCl-Ringer (time = 0 min); (*B*) After changing superfusion solution to K-cyclamate Ringer (time = 2 min); (*C*) After return to KCl-Ringer (time = 4.5 min).

(ΔI_{out}% = 27.7 ± 4.2%, n = 5, p < 0.01) after cyclamate washout with NaCl- or KCl-Ringer.

Effect of barium in single M-1 cells. Fig. 8 shows the effect of addition of 2 mM $BaCl_2$ in the presence of KCl-Ringer. Ba^{2+} reduces G_{cell} by 48 ± 4% from 5.36 ± 1.22 nS to 2.60 ± 0.57 nS (n = 14, p < 0.01). After washout of Ba^{2+}, G_{cell} recovered to 4.39 ± 0.94 nS (n = 14). Fig. 9 shows current traces from voltage step protocols and the corresponding I/V plots in control, presence of barium and after washout. The I/V plots represent late current readings, between 387 and 397 ms into the pulse. Barium reduces the inward conductance much more than the outward conductance. Whole cell conductance shows an inversion point at a V_{hold} of −60 mV which is compatible with the known voltage dependence of the barium blockade in K-channels. After washout of barium (Figs. 8 and 9), the inward conductance recovers almost completely and the I/V plot in symmetrical potassium shows again a small degree of inward rectification.

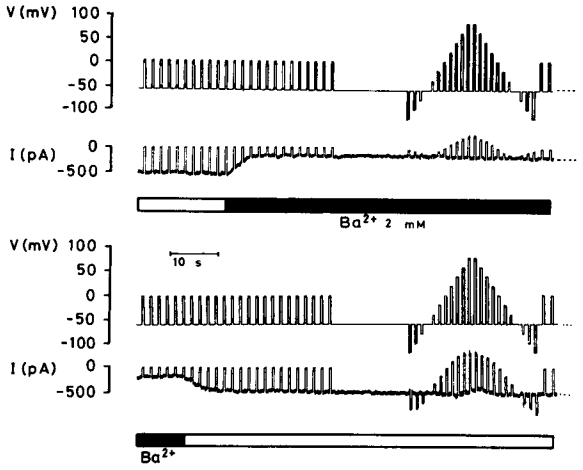

FIGURE 8. Effect of 2 mM barium. Continuous whole-cell current recording in symmetrical KCl-Ringer from a single M-1 cell, 1 d after seeding. Barium present as shown by the solid bar. Other conventions as in Fig. 3.

Effect of glibenclamide in single M-1 cells. The effect of glibenclamide, a known inhibitor of ATP-sensitive K-channels, was tested on G_{cell} in the presence of K-Ringer. Fig. 10 shows that glibenclamide (500 μM) reduces G_{cell} by 64%. Subsequent addition of 2 mM $BaCl_2$ during the same experiment reduces G_{cell} by 52% (not shown). In similar experiments, the average reduction of G_{cell} by 500 μM glibenclamide is 71 ± 2%, from 3.79 ± 0.74 nS to 1.01 ± 0.17 nS (n = 12, p < 0.01). A smaller effect was seen in two experiments using 100 μM glibenclamide in which G_{cell} was reduced by 27 and 14%. Washout of glibenclamide usually results in a partial recovery of the conductance. G_{cell}, after glibenclamide washout, averages 2.64 ± 0.53 nS (n = 11), which is less than the conductance before the application of glibenclamide. Fig. 11 shows current traces and I/V plots obtained in control K-Ringer, during 500 μM glibenclamide, and after washout. In contrast to barium, glibenclamide inhibits both inward and outward currents. It is noteworthy that glibenclamide abolishes the time-dependent portion of the outward current (n = 2, Fig. 11 *B*).

Two experiments were performed in which 500 μM glibenclamide was applied to 1-d old M-1 cells bathed in control NaCl-Ringer. In the first experiment, glibenclamide depolarized V_m from −41.5 to −30.0 mV and reduced G_{cell} by 78% from 3.83 nS in control Na-Ringer to 0.83 nS in the presence of glibenclamide. In the second

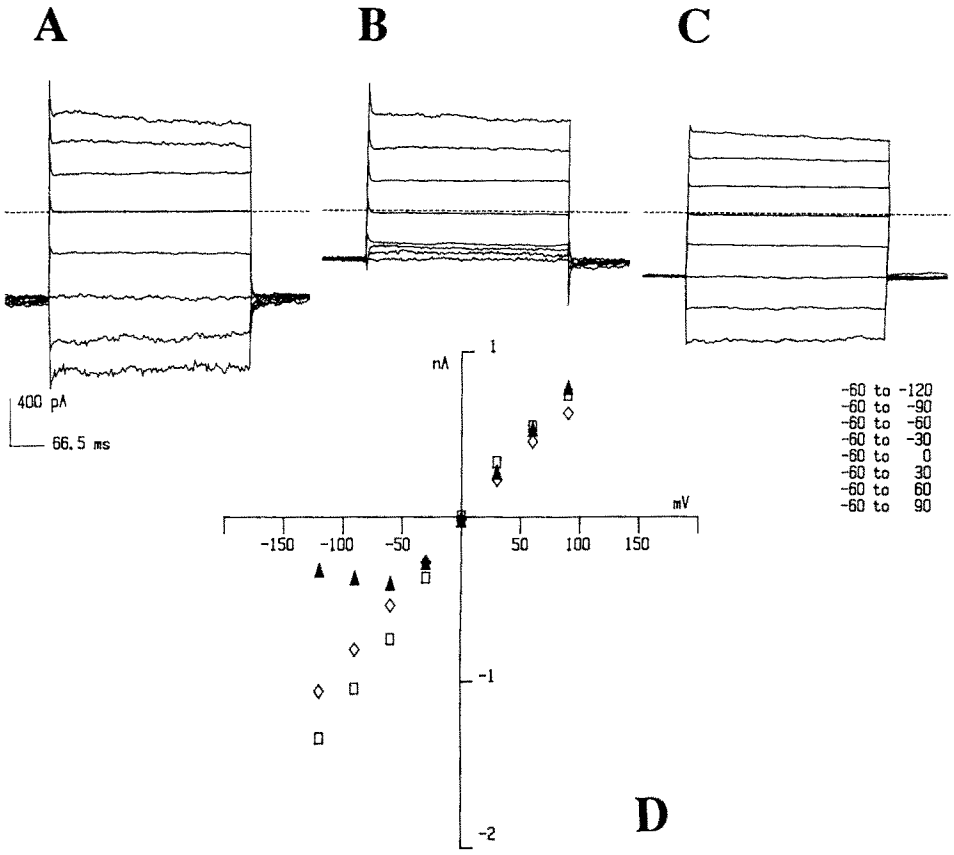

FIGURE 9. Whole-cell current traces (*A–C*) and I/V plots (*D*) obtained from voltage step protocols on a single M-1 cell in symmetrical KCl-Ringer, 1 d after seeding. (*A*) Control (time = 0 min); (*B*) 2 mM Ba^{2+} (time = 2 min); (*C*) washout of Ba^{2+} (time = 4.3 min); (*D*) I/V plots of readings 387–397 ms into the pulse, control (*open squares*), during Ba^{2+} (*solid triangles*), and washout of Ba^{2+} (*open diamonds*).

Whole-Cell Current Measurements in Confluent M-1 Monolayers

Effect of amiloride in confluent M-1 cells. In contrast to single cells in which amiloride had only minor effects, application of amiloride to confluent M-1 monolayer cultures causes a rapid hyperpolarization (Fig. 12). I/V plots obtained from whole cell membrane currents measured during a similar experiment are shown in Fig. 13 *A*.

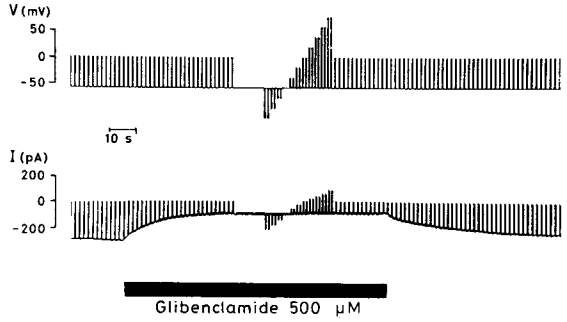

FIGURE 10. Effect of 500 μM glibenclamide. Continuous whole-cell current recording from a single M-1 cell in symmetrical KCl-Ringer, 1 d after seeding. Glibenclamide present as shown by the solid bar. Other conventions as in Fig. 3.

Amiloride reduces the whole cell conductance and shifts the reversal potential to the left (Fig. 13 *A*) in agreement with the hyperpolarization of V_m. The currents from voltage protocols were averaged before the application of amiloride and after amiloride washout. The amiloride-sensitive current is calculated by subtracting the current measured in the presence of amiloride from the corresponding average control current. Fig. 13 *B* illustrates the average amiloride-sensitive currents from

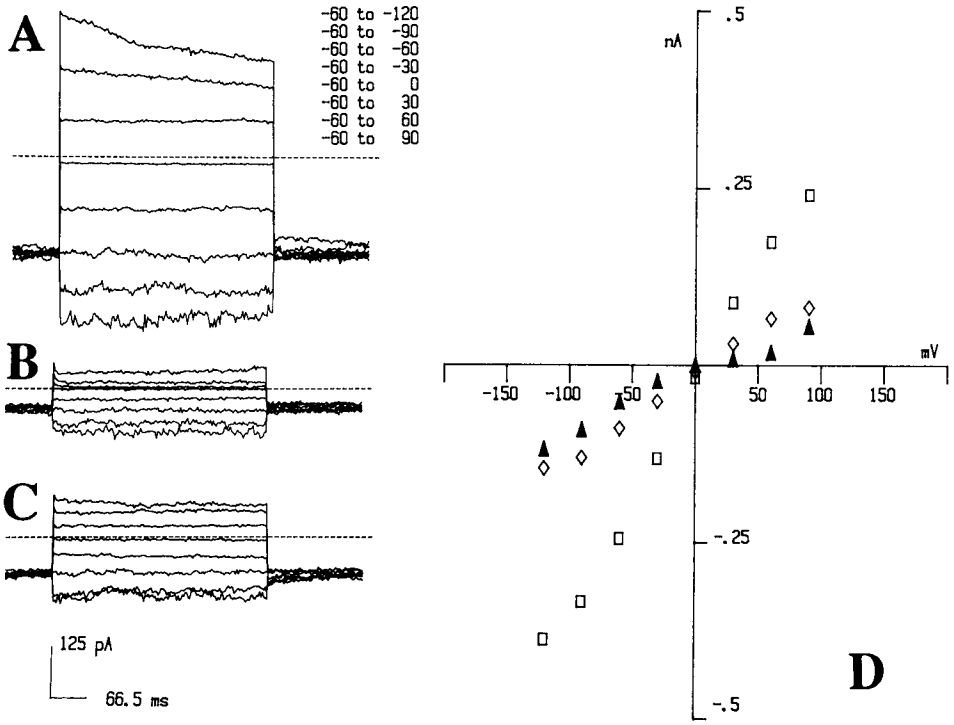

FIGURE 11. Whole-cell current traces (*A–C*) and I/V plots (*D*) obtained from voltage step protocols on a single M-1 cell in symmetrical KCl-Ringer, one day after seeding. (*A*) Control (time = 0 min); (*B*) 500 μM glibenclamide (time = 2.5 min); (*C*) washout of glibenclamide (time = 5 min); (*D*) I/V plots of readings 387–397 ms into the pulse, control (open squares), during glibenclamide (*solid triangles*), and washout of glibenclamide (*open diamonds*).

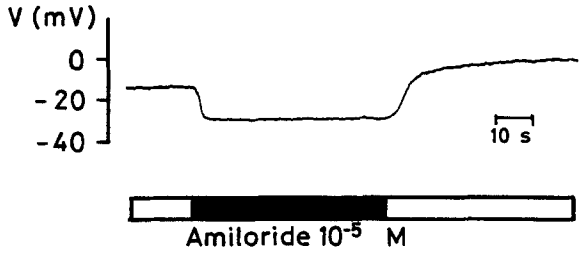

FIGURE 12. Effect of 10^{-5} M amiloride on membrane voltage (V) recorded in zero current clamp mode in a cell within a confluent M-1 monolayer, bathed in NaCl Ringer. Amiloride present as shown by the solid bar.

seven experiments similar to that shown in Fig. 13 *A*. Linear regression analysis of the average amiloride-sensitive currents yields a reversal potential at +62.4 ± 2.8 mV (n = 9), indicating a sodium to potassium selectivity ratio of ~15.

In a total of 10 experiments, amiloride 10^{-4} M (n = 2) or 10^{-5} M (n = 8) decreases G_{cell} of confluent M-1 cells by 31 ± 6% from 5.41 ± 1.06 nS to 3.61 ± 0.74 nS (n = 10, $p < 0.01$) and hyperpolarizes the membrane voltage from −21.9 ± 3.4 mV to −39.7 ± 3.0 mV (n = 10, $p < 0.01$). After washout of amiloride, G_{cell} recovers to 4.12 ± 0.69 nS (n = 10, not significantly different from control) and V_m depolarizes to −6.3 ± 3.1 mV, a value which is significantly more positive than the membrane voltage before the addition of amiloride (n = 10, $p < 0.001$).

Exposure of confluent M-1 cells to KCl-Ringer, barium, and glibenclamide. Changing the apical superfusion solution in M-1 monolayer cells from control NaCl-Ringer to

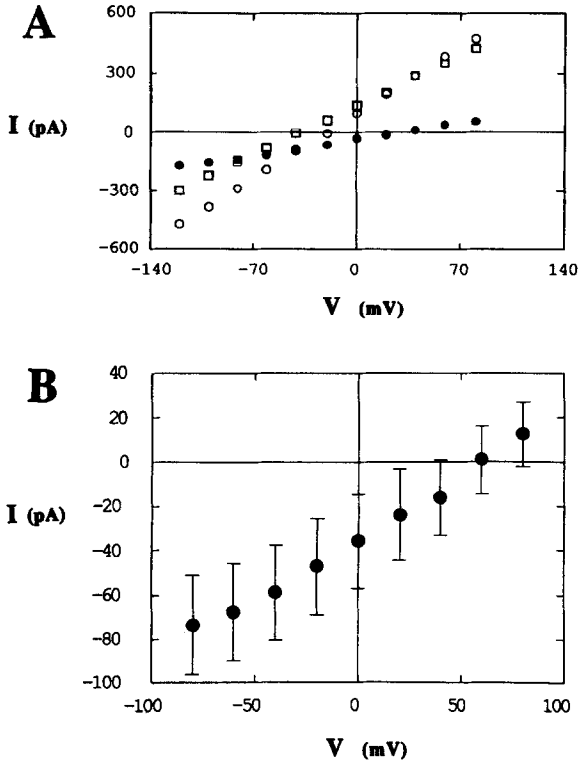

FIGURE 13. Effect of 10^{-5} M amiloride on whole-cell membrane current (I) in confluent M-1 cells. (*A*) I/V plots of currents in voltage step protocols. Average of whole-cell membrane currents before application and after washout of amiloride (*open circles*). 10^{-5} M amiloride (*open squares*). Amiloride-sensitive current (*solid circles*). (*B*) Average of amiloride-sensitive currents in seven experiments. Error bars show SEM.

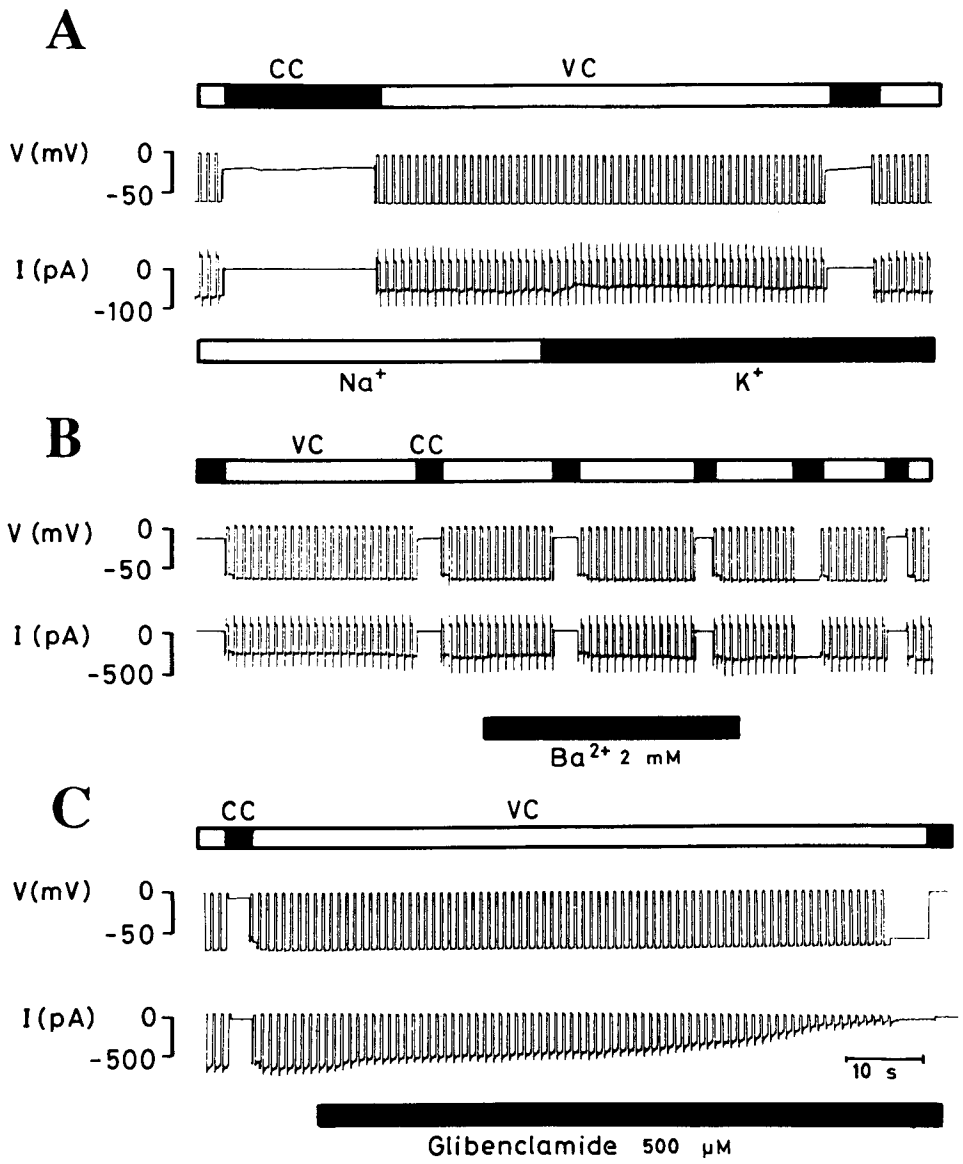

FIGURE 14. Continuous whole-cell recordings in confluent M-1 cells. (*A*) Changing from NaCl-Ringer (Na^+) to KCl-Ringer (K^+); (*B*) Effect of 2 mM Ba^{2+} in symmetrical KCl-Ringer; (*C*) Effect of 500 μM glibenclamide in symmetrical KCl-Ringer. Conventions as in Fig. 3. In *B* and *C*, upon returning to VC from CC, the voltage drop due to the series resistance was computed and digitally added back to the command voltage.

KCl-Ringer (Fig. 14*A*) did not induce the immediate increase in G_{cell} and the membrane voltage depolarization observed in single 1-d old M-1 cells. Instead, membrane voltage depolarization is modest (from -21.3 ± 6.0 mV to -15.4 ± 2.1 mV, $n = 8$) and develops slowly over time (Fig. 14*A*). In experiments similar to that

shown in Fig. 14 *A*, G_{cell} averages 4.78 ± 1.09 nS in a NaCl-Ringer superfusion solution and 4.13 ± 0.79 nS in KCl-Ringer (n = 8, not significantly different from control in paired t test).

Superfusion of M-1 monolayer cells with KCl-Ringer containing 2 mM $BaCl_2$ did not significantly affect G_{cell} as shown in a typical trace in Fig. 14 *B*. In similar experiments G_{cell} averages 6.47 ± 0.61 nS before the application of barium, 5.57 ± 0.61 nS in the presence of barium (n = 6, not significantly different from control in paired t test), and 5.63 ± 0.64 nS after washout. In contrast, application of 500 μM glibenclamide reduces G_{cell} in confluent M-1 cells by 83 ± 2% from 4.24 ± 1.08 nS to 0.58 ± 0.11 nS (n = 8, $p < 0.01$). A typical experiment is shown in Fig. 14 *C*. Note, that the time course of the glibenclamide action is much slower in the monolayer M-1 cells as compared to the glibenclamide effect in single M-1 cells (compare Fig. 10). The time delay between addition of glibenclamide to the superfusion solution and the maximal glibenclamide effect, was significantly longer in the monolayer cultures (153 ± 24 s, n = 8 versus 28 ± 3 s, n = 12, $p < 0.01$). In three out of eight experiments with confluent M-1 cells, the glibenclamide effect was partially reversible. The washout in these experiments was much slower than that observed with single M-1 cells (Fig. 10).

DISCUSSION

Cell Morphology

In the present study we show that M-1 cells grown on permeable support form an epithelial monolayer of polarized cells with tight junctions, apical microvilli, and central cilia. The EM-studies indicate the presence of a uniform cell type and give no indication of morphologically distinguishable subpopulations of cells in the M-1 cell line. When grown on nonpermeable support, M-1 cells form 'domes' which are evidence for active transepithelial reabsorption of solutes and water across the monolayer. M-1 cell monolayers grown on glass, as used in the patch clamp experiments, are remarkably differentiated. They possess tight junctions, microvilli and central cilia. A central cilium is a characteristic feature of in vivo cortical collecting duct principal cells.

Transepithelial Measurements

The development of transepithelial ion gradients across M-1 cell monolayers demonstrates the presence of active amiloride-sensitive sodium reabsorption and active potassium secretion. These are characteristic transport features of the cortical collecting duct in vivo and were preserved in the M-1 cells throughout the passages used. Transepithelial resistance and transepithelial potential difference across M-1 monolayers are in the same range as previously reported for isolated perfused cortical collecting ducts of rabbits (O'Neil and Boulpaep, 1979, 1982) and rats (Reif, Troutman, and Schafer, 1984). The results of the present study are also in good agreement with the previous findings reported on the M-1 cell line (Stoos et al., 1991; Fejes-Tóth and Naray Fejes-Tóth, 1992).

Patch Clamp Experiments in Single and Confluent M-1 Cells

Patch clamp experiments using the whole-cell configuration were performed in single M-1 cells and in M-1 cells within a confluent epithelial monolayer. Interpretation of the remarkably different results from single versus confluent cells is complicated by the different geometry and its impact on effectiveness of solution exchanges, membrane potential, and current distribution in patch clamping.

Solution exchange. In the single cells, epithelial polarization has not yet occurred. No tight junctions have developed and both apical and basolateral membrane domains are presumably readily accessible to solution exchanges. The configuration for cells patched in a confluent monolayer is more complex. The superfusion solution

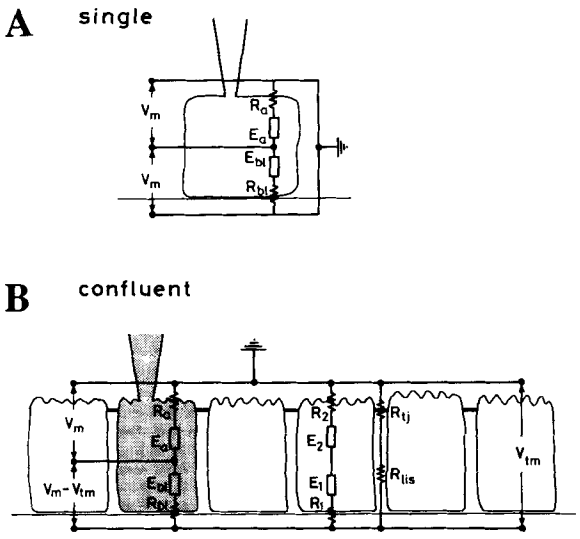

FIGURE 15. Equivalent circuit model for whole-cell patch clamp recording in (*A*) single cells and (*B*) confluent cells forming a polarized epithelium with tight junctions. V_m = cell membrane potential difference (cytosol − ground), V_{tm} = *trans*-monolayer potential difference (ground − basal extracellular space), R_a = apical membrane resistance of patched cell, R_{bl} = basolateral membrane resistance of patched cell, E_a = e.m.f. at apical membrane of patched cell, E_{bl} = e.m.f. at basolateral membrane of patched cell, R_1 = aggregate basolateral membrane resistance of cells within monolayer, R_2 = aggregate apical membrane resistance of cells within monolayer, R_{tj} = aggregate tight junction resistance of monolayer, R_{lis} = aggregate lateral and basal extracellular space resistance of monolayer, E_1 = equivalent e.m.f. of the basolateral membranes of cells within monolayer, E_2 = equivalent e.m.f. of apical membranes of cells within monolayer.

primarily affects the apical surface of the cell membrane. Test solutions or drugs applied may or may not reach the basolateral membrane, depending on the permeability of the tight junctions and on the degree of access to the basolateral spaces at the edges of the monolayer. Thus, the presence or lack of effects upon solution exchange in confluent monolayers is more difficult to interpret than in single cells.

Membrane potential measurements. In single M-1 cells apical and basolateral membrane domains are electrically shunted by the surrounding bath solution. Transmembrane potential (V_m), as measured in whole-cell experiments by the zero current clamp mode, is therefore uniform over the entire cell membrane area with respect to the bath solution which is grounded (Fig. 15*A*). In confluent cells, apical

and basolateral membranes are not as completely shunted as in single cells, and a transmonolayer potential difference (V_{tm}) can develop between the apical bath and the basolateral extracellular spaces. The magnitude of V_{tm} will depend on the relative magnitude of the apical Na permeability, electrogenic sodium transport, the tight junctional R_{tj} and lateral interspace resistances R_{lis}, transcellular resistances ($R_1 + R_2$) (Fig. 15 *B*) and the leak conductances. V_{tm} corresponds to V_{te} measured across M-1 cells grown on permeable supports but is opposite in sign, because for the patch clamp experiments the reference bath electrode is on the apical side. Transmembrane potential (V_m) measured in whole-cell experiments on confluent cells is referred to ground in the apical bath and equals the apical membrane potential difference. However, as shown in Fig. 15 *B* the basolateral membrane potential difference equals V_m minus V_{tm}.

The more negative values of V_m in single versus confluent cells in this study confirm the postulate of a finite transmonolayer potential difference V_{tm} in M-1 cells grown on glass cover slips. Indeed, the difference between V_m measured in single cells and V_m in confluent cells (Table IV) amounts to 25.9 mV. If the basolateral membrane

TABLE VI

Comparison of Conductance Changes Induced by Various Maneuvers in Single and Confluent M-1 Cells

Maneuver	Single cells	Confluent cells
Amiloride (10^{-5}–10^{-4} M) in NaCl-Ringer $(G^{145Na}-G^{145Na+AMI})/G^{145Na}$ =	0.09 ± 0.04 (n = 9)[ns]	0.31 ± 0.06 (n = 10)
KCl-Ringer vs. NaCl-Ringer $(G^{145K}-G^{145Na})/G^{145K}$ =	0.49 ± 0.04 (n = 19)	−0.13 ± 0.08 (n = 8)[ns]
Barium (2 mM) in KCl-Ringer $(G^{145K}-G^{145K+Ba})/G^{145K}$ =	0.48 ± 0.04 (n = 14)	0.13 ± 0.06 (n = 6)[ns]
Glibenclamide (500 μM) in KCl-Ringer $(G^{145K} - G^{145K+Glib})/G^{145K}$ =	0.71 ± 0.02 (n = 12)	0.83 ± 0.02 (n = 9)

[ns]Not significantly different from zero.

potential does not differ appreciably between single and confluent cells, the value of 25.9 mV is an approximate estimate of the transmonolayer potential (V_{tm}). This is consistent with the observed average transepithelial potential V_{te} = −28.8 mV (Table II) in M-1 cells on permeable support.

Whole-cell current distribution. Voltage clamping of single cells results in a spatially uniform voltage step across both apical and basolateral membrane domains. Current density across different membrane domains will vary inversely to the local transverse resistance of the domains. Thus, whole-cell G_{cell} reflects the sum of all apical and basolateral conductances (Fig. 15 *A*). In confluent cells, the whole-cell current flow to ground divides in an apical and a basolateral component. The apical current flows across a single apical membrane resistance (R_a) whereas the basolateral current traverses the basolateral membrane (R_b), the basolateral extracellular spaces (R_{lis}) and the tight junctional resistance(s) (R_{tj}) (Fig. 15 *B*). Assuming that wide basolateral extracellular spaces offer little resistance, the basolateral membrane of an individual cell within a confluent monolayer is effectively shunted via the many

surrounding tight junctional resistances in parallel. Because the basolateral resistance of an individual cell within a monolayer is probably high compared to the aggregate shunt resistance of the entire monolayer, any error in the basolateral voltage clamp introduced by series resistances becomes negligible. We therefore assume that in whole-cell recording of confluent cells the current distribution between the apical and basolateral domains does not differ from that in single cells and that the measured conductance G_{cell}, again reflects the sum of all apical and basolateral conductances. However, for the basolateral membrane the zero current potential (E_{rev}) in an I/V plot is shifted by the transmonolayer potential difference (Fig. 15 *B*).

The preceding considerations assume that no electrical coupling occurs between neighboring cells. Morphological evidence in M-1 cells does not support the presence of gap-junctional communication between the cells grown on glass cover slips. Instead, wide intercellular spaces exist, which do not facilitate close cell to cell contact. Furthermore, any considerable degree of cell-to-cell coupling during whole-cell recording of confluent cells seems unlikely, because cell capacitance measurements did not differ between single and confluent M-1 cells (Table IV). Our findings are in agreement with a recent study in which whole-cell currents were measured in principal cells of split-open rat cortical collecting tubules. The absence of carboxyfluorescein diffusion between adjacent principal cells was interpreted as lack of coupling, and the similarity of the calculated and measured capacitance values also supported the presumption that whole-cell currents arose from single principal cells (Frindt et al., 1990). Thus, we assume that whole cell transmembrane current flow in confluent M-1 monolayers is confined to the plasma membrane of an individual cell.

Whole-cell conductance. G_{cell} was found to be 2.6 times higher in confluent cells than in single cells (Table IV). The equivalent circuit considerations of Fig. 15, *A* and *B*, demonstrate that these differences in G_{cell} should not result from spatial differences in current distribution. Thus, differences in G_{cell} may originate from differences in the apical and/or basolateral membrane conductances.

Sodium Conductance

Amiloride hyperpolarizes V_m by only 3.0 mV in single M-1 cells but by 17.8 mV in confluent M-1 cells. In Table VI the fractional contribution of the amiloride-sensitive conductance to G_{cell} is compared between single and confluent cells. Mean values of the conductance changes, normalized to the reference G_{cell} in NaCl-Ringer, show that the amiloride-sensitive conductance does not differ from zero in single cells, but constitutes 31% of the G_{cell} in confluent cells. As discussed above, the conductance measured in single cells and in confluent cells reflects in both cases the sum of all apical and basolateral conductances. Thus, the higher amiloride-sensitive fraction of G_{cell} in the confluent cells compared to the single cells is not caused by a different current distribution.

Single M-1 cells derived from confluent monolayer cultures express 24 h after seeding, a total G_{cell} reduced by 62%, as compared to confluent M-1 cells (Table IV). Since we used trypsin to passage the M-1 cells, the reduction of G_{cell} may in part be due to proteolytic destruction of channel proteins and to internalization of channels in intracellular compartments. Garty and Edelman (1983) have reported that trypsin decreases short-circuit current of the toad urinary bladder to 50% of the initial value

by an amiloride-sensitive trypsinization of apical sodium channels. The effect was poorly reversible and 1 h after termination of trypsin treatment short circuit current was still decreased to 60% of the initial value. Whereas in the toad urinary bladder experiments, trypsin presumably only acts on the apical surface, trypsin can reach both apical and basolateral surfaces during separation of M-1 cells. Because trypsin is rather nonspecific, it is unlikely that it selectively destroys only sodium channels, rather than attack all channel proteins in the cell membrane. During the subsequent 24-h recovery period, sodium channels are slow to reappear and G_{cell} of single cells is initially dominated by a potassium and chloride conductance. The difference in the conductance properties of single versus confluent M-1 cells may indicate that the M-1 cells have to form a polarized epithelium in order to express amiloride-sensitive sodium channels. It is tempting to speculate that the apical sorting and insertion of sodium channels may require special cell-cell contact signals and assembly of a polarized membrane-cytoskeleton (Rodriguez-Boulan and Nelson, 1989).

The average amiloride-sensitive whole-cell current in the confluent cells has a reversal potential of $\sim +60$ mV which indicates a sodium to potassium permeability ratio of ~ 15 similar to the selectivity reported in A6 cells and in rat cortical collecting tubule (Garty and Benos, 1988). The amiloride-sensitive G_{cell} in confluent M-1 cells of 1.8 nS/cell is an intermediate value between the 6.0 nS/cell reported in cortical collecting duct cells of rats on a low sodium diet and the 0.06 nS/cell in rats on control diet (Frindt and Palmer, 1990).

The presence of an apical amiloride-sensitive sodium conductance probably also explains the 25.9-mV difference in resting membrane voltage between single and confluent M-1 cells. The disparity is similar in size to the amiloride-sensitive transepithelial voltage difference in M-1 cells grown on permeable support. According to the equivalent circuit of Fig. 15 *B*, V_m measured by whole-cell recording in confluent cells corresponds to the apical membrane potential. In the absence of amiloride the sodium conductance depolarizes V_m. Amiloride abolishes the transmonolayer potential difference and hyperpolarizes V_m across the apical membrane. The membrane voltage response observed in the confluent cells upon application of amiloride is in good agreement with this interpretation and with the electrical circuit model depicted in Fig. 15 *B*.

Nonselective Cation Conductance

Single channel patch-clamp studies have demonstrated the presence of nonselective cation channels in various collecting duct cells (Light, McCann, Keller, and Stanton, 1988; Laskowski, Christine, Gitter, Beyenbach, Gross, and Frömter, 1990; Ling, Hinton, and Eaton, 1991), including M-1 cells (Ahmad, Korbmacher, Segal, Cheung, Boulpaep, and Barnstable, 1992). The nonselective cation channel in the inner medullary collecting duct has been shown to be sensitive to submicromolar concentrations of extracellular amiloride (Light et al., 1988) and has been suggested to play a role in sodium reabsorption (Light, Schwiebert, Karlson, and Stanton, 1989). In confluent M-1 cells, the amiloride-sensitive whole-cell current is highly sodium selective (see above). Hence, an amiloride-sensitive nonselective cation channel is unlikely to contribute to the amiloride-sensitive conductance observed in M-1 cells. Furthermore, nonselective cation channel activity in M-1 cells is rarely seen in

cell-attached patches and nonselective cation channel activity in inside-out patches is abolished in nominally calcium-free Ringer containing 1 mM EGTA (Korbmacher, Segal, and Boulpaep, 1992; Ahmad et al., 1992). Because in the whole-cell experiments, the M-1 cells were dialyzed with nominally calcium-free Ringer containing 1 mM EGTA, we presume that nonselective cation channels did not contribute to the whole-cell conductance.

Potassium Conductance

In single M-1 cells the membrane potential is dominated by a K^+-conductance, as evidenced by the negative V_m in a NaCl-Ringer bath, and by the large membrane depolarization and doubling of G_{cell} upon exposure to external KCl-Ringer. The dependence of the membrane potential on the potassium conductance is further demonstrated by the close correlation among different cells between the negative V_m and the sensitivity of G_{cell} to high K solutions (Fig. 4). The average sensitivity of single cells to high K solutions can be estimated from the fractional conductance change between 145 mM K-Ringer and 145 mM Na-Ringer, normalized to the total conductance measured in 145 mM K-Ringer. As shown in Table VI, the fractional conductance $(G^{145K} - G^{145Na})/G^{145K}$ in single cells is 0.49.

The whole-cell conductance in the presence of symmetrical potassium solutions is barium-sensitive and the barium block was voltage dependent as expected for barium. The fractional conductance $(G^{145K} - G^{145K+Ba})/G^{145K}$ in single cells is 0.48, indicating that about half of it is given by barium-sensitive K channels (Table VI). Barium-sensitive Ca-dependent maxi-K channels have been found in the apical membrane of cortical collecting duct cells (Hunter et al., 1984; Frindt and Palmer, 1987; Gitter, Beyenbach, Christine, Gross, Minuth, and Frömter, 1987). However, because in our whole-cell experiments in M-1 cells, the pipette solution was calcium free and in addition contained 1 mM EGTA, we do not expect any calcium-activated maxi-K channel to contribute to the observed barium-sensitive conductance. The barium-sensitive conductance of M-1 cells has to be mediated by a different type(s) of K-channel.

A novel finding in this study is the presence of a glibenclamide-sensitive conductance in M-1 cells. The sulfonylurea drug glibenclamide is believed to be a specific blocker of ATP-sensitive K-channels in a variety of tissues (Ashcroft, 1988). The average glibenclamide-sensitive fractional conductance in single cells is 71% versus 83% in confluent cells (Table VI). The glibenclamide concentrations used in the present study are high compared to the concentrations used on human pancreatic islet cells. However, the sensitivity of ATP-sensitive K^+ channels towards sulfonylurea derivatives is known to vary considerably among different tissues (Ashcroft, 1988). In addition, glibenclamide at high concentrations may no longer act exclusively on ATP-sensitive K-channels. Wangemann, Wittner, Di Stefano, Englert, Lang, Schlatter, and Greger (1986) reported that glibenclamide inhibits the chloride conductance in thick ascending limb with a K_i of 80 μM. A recent report on fibroblasts transfected with CFTR shows that glibenclamide inhibits whole-cell CFTR chloride currents with a K_i of 20 μM (Sheppard and Welsh, 1992). Thus, it is possible that the conductance decrease observed in M-1 cells in the presence of glibenclamide is not due to inhibition of ATP-sensitive K-channels only, but also to inhibition of a chloride

conductance. This is supported by our finding that the time-dependent component of the outward current, attributed to a chloride conductance (see below), disappears in the presence of glibenclamide (Fig. 11). However, taking into account the considerable overlap between the K-sensitive, the Ba^{2+}-sensitive and the glibenclamide-sensitive fractional conductance in single cells (Table VI), the major glibenclamide effect in M-1 cells should be due to inhibition of K-channels.

A small-conductance ATP-sensitive K-channel has previously been demonstrated in the apical membrane of rat cortical collecting duct cells and is believed to mediate potassium secretion and its regulation (Wang and Giebisch, 1991*a,b*). In inside-out patches this channel can be blocked by sulfonylurea drugs (Wang, personal communication). Because M-1 cells secrete potassium, a similar channel may exist in their apical membrane. However, our whole-cell experiments give no indication for the presence of an appreciable apical K-conductance in confluent M-1 cells because superfusion with 2 mM barium has no significant effect (Table VI). The relative size of the glibenclamide effect is similar in single and confluent M-1 cells (Table VI). In contrast, the slower time course of the glibenclamide effect in confluent cells suggests a basolateral action of the lipophilic drug. A basolateral ATP-sensitive K-channel reported in the rat proximal tubule also requires relatively high concentrations of glibenclamide for inhibition with a K_i of 250 μM (Tsuchiya, Wang, Giebisch, and Welling, 1992). It is tempting to speculate that M-1 cells possess an ATP-sensitive K-channel in their basolateral membrane similar to that observed in rabbit proximal tubule. In conclusion, the glibenclamide effect observed in the present whole-cell study is compatible with the presence of basolateral ATP-sensitive K-channels in M-1 cells.

Chloride Conductance

A chloride component of the whole-cell conductance was detected as a deactivating outward current during large depolarizing voltage pulses. This decaying current is attributed to a chloride conductance because it is insensitive to extracellular cation replacement and abolished by extracellular chloride removal. Furthermore, the deactivating outward current is inhibited by glibenclamide, which has been shown to block chloride channels in thick ascending limb (Wangemann et al., 1986) and CFTR chloride channels (Sheppard and Welsh, 1992). The chloride conductance is also present at the holding potential of −60 mV, as evidenced by the instantaneous peak current when the voltage is stepped from −60 mV to +60 mV or +90 mV, and by the recovery of a tail current upon returning to −60 mV. The instantaneous contribution of the chloride conductance to the outward current averages 24%, assuming a complete deactivation after 400 ms. However, a time constant of relaxation of 179 ms predicts that at the end of a 400 ms voltage step the current should have decayed to within 10.7% of the initial value. The absolute magnitude of the deactivating chloride current of 103.6 pA/cell may therefore be underestimated by ~10%.

In symmetrical KCl-Ringer the instantaneous whole-cell current-voltage plots are mostly linear or slightly outward rectifying, whereas the steady state current-voltage plots at 400 ms show inward rectification. Hence, the difference current exhibits outward rectification. The hypothesis that the underlying chloride conductance is an

outward rectifier is further supported by the calculated conductance ratio $\Delta G_{out}/\Delta G_{in} = 2.4$ obtained from deactivating currents and tail currents.

Single chloride channels and whole cell chloride conductances have been found to rectify in the outward direction in airway epithelia (Welsh, 1986; Frizzell, Rechkemmer, and Shoemaker, 1986). A remarkable similarity of the M-1 cell chloride conductance with airway epithelium channels is the time-dependent deactivation upon depolarization. The time constant of conductance decay in M-1 cells of 179 ms is in good agreement with the time course of whole-cell current decay reported for airway epithelial cells. Finally, the outward to inward conductance ratio of 2.4 in M-1 cells compares favorably with the ratio of ~3 between the conductance at −120 mV and +80 mV observed in airway epithelium (McCann, Li, and Welsh, 1989).

The chloride channel of airway epithelium is located on the apical membrane. Our findings argue against an apical site for the chloride conductance in M-1 cells. The chloride conductance component in single M-1 cells is abolished by external chloride removal. In contrast, in confluent cells, superfusion of the apical membrane with cyclamate solutions did not abolish the time-dependent deactivation (data not shown). A basolateral chloride conductance in M-1 cortical collecting duct cells could contribute to chloride reabsorption and possibly volume regulation (Sansom et al., 1990; Strange, 1991). Chloride reabsorption has previously been shown to occur in M-1 cells grown on permeable support (Stoos et al., 1991) and is consistent with the decrease in total cation concentration in the apical compartment observed in the present study, suggesting parallel sodium and chloride reabsorption. The M-1 cells may thus provide a useful model to further investigate the role of chloride channels in CCD function.

Conclusion

Transepithelial measurements and ultrastructure demonstrate that M-1 cells share functional and morphological properties of principal cells in vivo and provide a useful model to study cortical collecting duct function in vitro. Whole-cell conductance differences observed between single and confluent M-1 cells are not due to electrical circuit differences. Thus, an amiloride-sensitive, sodium-selective conductance detected in confluent cells indicates that confluent cells express more sodium channels in their apical membrane than single cells do in their whole cell membrane. Cell-to-cell contact and formation of tight junctions may be required for sodium channel insertion in the apical membrane. Application of external KCl or barium reveals the presence of a K-conductance in single but not in confluent M-1 cells. Thus, under our experimental conditions, confluent cells lack a significant apical K-conductance, whereas KCl and barium may have limited access to the basolateral membrane of confluent cells. In contrast, the lipophilic drug glibenclamide, a known inhibitor of ATP-sensitive K-channels, causes a comparable inhibition of the whole-cell conductance in single and confluent M-1 cells. The slower time course of the glibenclamide effect in confluent cells suggests a basolateral location of ATP-sensitive K-channels in M-1 cells. Finally, a chloride component of the whole-cell conductance has been detected as a deactivating outward current during large depolarizing voltage pulses. This chloride conductance is glibenclamide-sensitive and probably located in the basolateral membrane of the M-1 cells.

We thank Thomas A. Ardito for expert electron microscopy and Marianne Koch for help in preparing the ink drawings.

This work was supported by grants DK-13844 and DK-17433 from the National Institutes of Health, a Forschungsstipendium of the Deutsche Forschungsgemeinschaft (DFG grant Ko 1057/1-2) and a Brown-Coxe fellowship from Yale University to C. Korbmacher, and a Burroughs Wellcome Fund/National Kidney Foundation Research Fellowship to A. S. Segal.

Original version received 9 September 1992 and accepted version received 12 June 1993.

REFERENCES

Ahmad, I., C. Korbmacher, A. S. Segal, P. Cheung, E. L. Boulpaep, and C. J. Barnstable. 1992. Mouse cortical collecting duct cells show nonselective cation channel activity and express a gene related to the cGMP-gated rod photoreceptor channel. *Proceedings of the National Academy of Sciences, USA.* 89:10262–10266.

Ashcroft, F. M. 1988. Adenosine 5'-triphosphate-sensitive potassium channels. *Annual Review of Neuroscience.* 11:97–118.

Bello-Reuss, E., and M. R. Weber. 1987. Electrophysiological studies of primary cultures of rabbit distal tubule cells. *American Journal of Physiology.* 252:F899–F909.

Fejes-Tóth, G., and A. Náray-Fejes-Tóth. 1992. Differentiation of renal β-intercalated cells to α-intercalated and principal cells in culture. *Proceedings of the National Academy of Sciences, USA.* 89:5487–5491.

Frindt, G., and M. B. Burg. 1972. Effect of vasopressin on sodium transport in renal cortical collecting tubules. *Kidney International.* 1:224–231.

Frindt, G., and L. G. Palmer. 1987. Ca-activated K channels in the apical membrane of mammalian CCT and their role in K secretion. *American Journal of Physiology.* 252:F458–F467.

Frindt, G., and L. G. Palmer. 1989. Low conductance K channels in apical membrane of rat cortical collecting tubule. *American Journal of Physiology.* 256:F143–F151.

Frindt, G., H. Sackin, and L. G. Palmer. 1990. Whole-cell currents in rat cortical collecting tubule: low-Na diet increases amiloride-sensitive conductance. *American Journal of Physiology.* 258:F562–F567.

Frizzell, R. A., G. Rechkemmer, and R. L. Shoemaker. 1986. Altered regulation of airway epithelial cell chloride channels in cystic fibrosis. *Science.* 233:558–560.

Garty, H., and D. J. Benos. 1988. Characteristics and regulatory mechanisms of the amiloride-blockable Na^+ channel. *Physiological Reviews.* 68:309–373.

Garty, H., and I. S. Edelman. 1983. Amiloride-sensitive trypsinization of apical sodium channels. *Journal of General Physiology.* 81:785–803.

Gitter, A. H., K. W. Beyenbach, C. W. Christine, P. Gross, W. W. Minuth, and E. Frömter. 1987. High-conductance K^+ channel in apical membranes of principal cells cultured from rabbit renal cortical collecting duct anlagen. *Pflügers Archiv.* 408:282–290.

Hamill, O. P., A. Marty, E. Neher, B. Sakmann, and F. J. Sigworth. 1981. Improved patch-clamp techniques for high-resolution current recording from cells and cell-free membrane patches. *Pflügers Archiv.* 391:85–100.

Handler, J. S., F. M. Perkins, and J. P. Johnson. 1980. Studies of renal cell function using cell culture techniques. *American Journal of Physiology.* 238:F1–F9.

Hunter, M., A. G. Lopes, E. L. Boulpaep, and G. Giebisch. 1984. Single channel recordings of calcium-activated potassium channels in the apical membrane of rabbit cortical collecting tubules. *Proceedings of the National Academy of Sciences, USA.* 81:4237–4239.

Koeppen, B. M., B. A. Biagi, and G. Giebisch. 1983. Intracellular microelectrode characterization of the rabbit cortical collecting duct. *American Journal of Physiology.* 244:F35–F47.

Korbmacher, C., A. S. Segal, and E. L. Boulpaep. 1992. Ion channels in a mouse cortical collecting duct cell line. *Renal Physiology and Biochemistry.* 15:180*a*. (Abstr.)

Korbmacher, C., A. S. Segal, G. Fejes-Tóth, G. Giebisch, and E. L. Boulpaep. 1991. Different expression of whole cell conductances in single and confluent M-1 mouse cortical collecting duct cells: effects of amiloride, barium and glibenclamide. *Journal of the American Society of Nephrology.* 2:743*a*. (Abstr.)

Laskowski, F. H., C. W. Christine, A. H. Gitter, K. W. Beyenbach, P. Gross, and E. Frömter. 1990. Cation channels in the apical membrane of collecting duct principal cell epithelium in culture. *Renal Physiology and Biochemistry.* 13:70–81.

Light, D. B., F. V. McCann, T. M. Keller, and B. A. Stanton. 1988. Amiloride-sensitive cation channel in apical membrane of inner medullary collecting duct. *American Journal of Physiology.* 255:F278–F286.

Light, D. B., E. M. Schwiebert, K. H. Karlson, and B. A. Stanton. 1989. Atrial natriuretic peptide inhibits a cation channel in renal inner medullary collecting duct cells. *Science.* 243:383–385.

Ling, B. N., C. F. Hinton, and D. C. Eaton. 1991. Potassium permeable channels in primary cultures of rabbit cortical collecting tubule. *Kidney International.* 40:441–452.

MacKay, K., L. J. Striker, S. Elliot, C. A. Pinkert, R. L. Brinster, and G. E. Striker. 1988. Glomerular epithelial, mesangial, and endothelial cell lines from transgenic mice. *Kidney International.* 33:677–684.

McCann, J. D., M. Li, and M. J. Welsh. 1989. Identification and regulation of whole-cell chloride currents in airway epithelium. *Journal of General Physiology.* 94:1015–1036.

Minuth, W. W., and W. Kriz. 1982. Renal collecting duct cells cultured as globular bodies and as monolayers. *Journal of Tissue Culture Methods.* 7:93–96.

O'Neil, R. G., and E. L. Boulpaep. 1979. Effect of amiloride on the apical cell membrane cation channels of a sodium-absorbing, potassium-secreting renal epithelium. *Journal of Membrane Biology.* 50:365–387.

O'Neil, R. G., and E. L. Boulpaep. 1982. Ionic conductive properties and electrophysiology of the rabbit cortical collecting tubule. *American Journal of Physiology.* 243:F81–F95.

Reif, M. C., S. L. Troutman, and J. A. Schafer. 1984. Sustained response to vasopressin in isolated rat cortical collecting tubule. *Kidney International.* 26:725–732.

Rodriguez-Boulan, E., and W. J. Nelson. 1989. Morphogenesis of the polarized epithelial cell phenotype. *Science.* 245:718–725.

Sansom, S. C., B.-Q. La, and S. L. Carosi. 1990. Double-barreled chloride channels of collecting duct basolateral membrane. *American Journal of Physiology.* 259:F46–F52.

Schlatter, E., and J. A. Schafer. 1987. Electrophysiological studies in principal cells or rat cortical collecting tubules: ADH increases the apical membrane Na^+ conductance. *Pflügers Archiv.* 409:81–92.

Sheppard, D. N., and M. J. Welsh. 1992. Effect of ATP-sensitive K^+ channel regulators on cystic fibrosis transmembrane conductance regulator chloride current. *Journal of General Physiology.* 100:573–591.

Spielman, W. S., W. K. Sonnenburg, M. L. Allen, L. J. Arend, K. Gerozissis, and W. L. Smith. 1986. Immunodissection and culture of rabbit cortical collecting tubule cells. *American Journal of Physiology.* 251:F348–F357.

Stoos, B. A., A. Náray-Fejes-Tóth, O. A. Carretero, S. Ito, and G. Fejes-Tóth. 1991. Characterization of a mouse cortical collecting duct cell line. *Kidney International.* 39:1168–1175.

Strange, K. 1991. Volume regulatory Cl^- loss after Na^+ pump inhibition in CCT principal cells. *American Journal of Physiology.* 260:F225–234.

Tsuchiya, K., W. Wang, G. Giebisch, and P. A. Welling. 1992. ATP is a coupling modulator of parallel Na,K-ATPase-K-channel activity in the renal proximal tubule. *Proceedings of the National Academy of Sciences, USA.* 89:6418–6422.

Wang, W., and G. Giebisch. 1991*a*. Dual effect of adenosine triphosphate on the apical small conductance K^+ channel of the rat cortical collecting duct. *Journal of General Physiology.* 98:35–61.

Wang, W., and G. Giebisch. 1991*b*. Dual modulation of renal ATP-sensitive K^+ channel by protein kinases A and C. *Proceedings of the National Academy of Sciences, USA.* 88:9722–9725.

Wangemann, P., M. Wittner, A. Di Stefano, H. C. Englert, H. J. Lang, E. Schlatter, and R. Greger. 1986. Cl^--channel blockers in the thick ascending limb of the loop of Henle: structure activity relationship. *Pflügers Archiv.* 407(Suppl. 2):S128–141.

Welsh, M. J. 1986. An apical membrane chloride channel in human tracheal epithelium. *Science.* 232:1648–1650.